Nanoscale

Cite this: *Nanoscale*, 2012, **4**, 4327

www.rsc.org/nanoscale

REVIEW

Nanobionics: the impact of nanotechnology on implantable medical bionic devices

G. G. Wallace,* M. J. Higgins, S. E. Moulton and C. Wang

Received 29th March 2012, Accepted 17th May 2012
DOI: 10.1039/c2nr30758h

The nexus of any bionic device can be found at the electrode–cellular interface. Overall efficiency is determined by our ability to transfer electronic information across that interface. The nanostructure imparted to electrodes plays a critical role in controlling the cascade of events that determines the composition and structure of that interface. With commonly used conductors: metals, carbon and organic conducting polymers, a number of approaches that promote control over structure in the nanodomain have emerged in recent years with subsequent studies revealing a critical dependency between nanostructure and cellular behaviour. As we continue to develop our understanding of how to create and characterise electromaterials in the nanodomain, this is expected to have a profound effect on the development of next generation bionic devices. In this review, we focus on advances in fabricating nanostructured electrodes that present new opportunities in the field of medical bionics. We also briefly evaluate the interactions of living cells with the nanostructured electromaterials, in addition to highlighting emerging tools used for nanofabrication and nanocharacterisation of the electrode–cellular interface.

1. Introduction

With the development of appropriate electrodes and electronics we have witnessed the development of devices that effectively interface biology and electronics: the bionic ear,[1] cardiac pacemakers,[2] vagus nerve stimulators for epilepsy control and pain management,[3] and devices that provide electrical stimulation for bone regrowth.[4] New areas of application such as the bionic eye[5] and the use of deep brain stimulators[6] for treatment of Parkinson's disease are being vigorously pursued. Critical in determining effective performance of all bionic devices is the chemical,

ARC Centre of Excellence for Electromaterials Science (ACES), Intelligent Polymer Research Institute, AIIM Facility, Innovation Campus, University of Wollongong, NSW 2522, Australia

G.G. Wallace

Gordon G. Wallace is Executive Research Director of the ARC Centre of Excellence for Electromaterials Science, an Australian Laureate Fellow and previously an ARC Federation Fellow. He is a Fellow of the Australian Academy of Science and the Australian Academy of Technological Sciences and Engineering. Professor Wallace's research interests include organic conductors, nanomaterials and electrochemical probe methods of analysis, and the use of these in the development of Intelligent Polymer Systems.

M. J. Higgins

Michael J. Higgins completed his PhD degree in Biology and Chemistry at the University of Melbourne, Australia, in 2003. He was a research fellow at the Centre for Research on Adaptive Nanodevices and Nanostructures (CRANN), Trinity College Dublin, Ireland in 2003–2007. Dr Higgins is currently an ARC Australian Research Fellow at the Intelligent Polymer Research Institute (IPRI), ARC Centre of Excellence for Electromaterials Science (ACES), University of Wollongong, Australia. His research interest is the cellular–material interface and application of scanning probe microscopy techniques to study biological systems at the nanoscale.

physical and electronic nature of the electrode–tissue interface that is established subsequent to implantation.[7] This interface is constructed through a cascade of protein and cellular interactions that are determined by the composition and physical structure of the materials that make up the implanted device.

It is now widely recognised that control of the nanodomain is critical in determining both protein–material[8] and cellular–material[9] interactions with many examples showing the effect of nanotopography on nerve,[10] muscle[11] or bone[12] regrowth. For example, Thapa *et al.* reported that poly(lactic-*co*-glycolic acid) (PLGA) nanostructures promoted greater adhesion of bladder smooth muscle cells compared with micron-structured controls.[13] Similar findings using a range of cells on PLGA nanostructured surfaces also suggested that nanotopography enhances cell adhesion and morphology.[14,15]

The electronic and mechanical properties of materials are also governed by nanostructure. For example, controlling the size of metal oxide particles in the nanodomain provides the ability to tune the electronic band gap, while control over the assembly process can result in structures with extraordinarily high surface area. These properties, in turn, control the ability to transport and store charge. In the area of organic conductors, the impact of control over nanostructure is particularly profound. For example, carbon nanotubes (CNTs) are amongst the strongest materials known with a theoretical tensile strength of 1.0 Tera Pascal and an elastic modulus of 462 to 546 GPa.[16] They also exhibit excellent electrical conductivity, with a resistivity between 10^{-4} and 10^{-6} Ω cm. The resistivity of a single graphene sheet is reported to be 10^{-6} Ω cm; this is less than the resistivity of silver. For organic conducting polymers (OCPs) such as polypyrrole, it is known that highly conducting regions can be found within nanodomains.[17,18] It has also been shown that the use of nanostructures enables very rapid electrochemical switching.[19]

Given the effect of nanostructure on the physical and biological properties of materials, it is not surprising that the fields of nanotechnology and medical bionics should merge to give birth to the integrated field of Nanobionics.

Here, we will review the most recent advances in nanostructured electromaterials that are of relevance to the field of medical bionics. We will review the interactions of proteins and living cells with nanostructured materials and the tools being used to study and visualise these events in the nanodomain. The clinical applications being pursued and progress to date will also be reviewed.

2. Medical bionics

A number of medical bionic devices have been developed in recent years. These include, for example, the cochlear implant (The Bionic Ear), the vagus nerve stimulator and visual prosthesis (The Bionic Eye).

The cochlear implant consists of platinum (Pt) electrode arrays integrated into a silicone rubber carrier.[20] The current design consists of a microphone to pick up sound, a speech transducer to translate the sound into a train of electrical impulses, and electrode housing that hosts the stimulating electrodes (Fig. 1). The sound is transmitted as electrical impulses that "communicate" with the ganglion nerve cells to enable hearing.

Vagus nerve stimulation (VNS) therapy developed by Cyberonics Inc. can be used for the treatment of refractory epilepsy[21,22] and treatment-resistant depression.[23,24] The VNS system utilizes platinum–iridium (Pt–Ir) cuff electrodes (3 mm in diameter, 1 mm in width and 250 μm thickness) that are placed around the vagus nerve in the left side of the neck of the patient. The system has two electrodes that are spaced approximately 5–6 mm apart. This spacing is critically important to achieve effective nerve stimulation. The electrodes are connected to the pulse generator hardware that sends mild electrical stimulation to the vagus nerve.

The first VNS implant for epilepsy was performed in 1988.[25] Since then, more than 60 000 patients worldwide have been treated with VNS providing a broad spectrum treatment for epilepsy,[26] with efficacy for both partial and generalized seizures.[27–29] The results of clinical trials have shown that VNS has efficacy that is comparable to the new anti-epilepsy drugs (AEDs), with continued improvement in seizure reduction for up to 2 years.[25] Recently, VNS has been used for management of treatment-resistant depression.[30] The clinical trials with 355 patients resulted in steadily increasing improvement with full benefit attained after 6–12 months treatment.

Vision bionics has recently attracted significant attention. An electrode is placed along the optic neural circuitry to effect visual percepts in blind subjects, including stimulation of existing

S. E. Moulton

Associate Professor Simon Moulton obtained his Ph.D. in 2002 from the University of Wollongong. In 2009 he was awarded the Australian Research Council Queen Elizabeth II Fellowship to develop novel drug delivery systems. He is currently Associate Program Leader with in ACES Bionics program working on developing conducting biomaterials for bionic applications for drug delivery as well as nerve, muscle, and bone regeneration.

C. Wang

Caiyun Wang obtained her BSc from Shandong Normal University in 1991 and MSc from Nankai University in 1994. She got her PhD in Materials Engineering from the University of Wollongong in 2004. She is a research fellow in the Intelligent Polymer Research Institute. Her current research interest is conducting polymer-based flexible, wearable or implantable batteries.

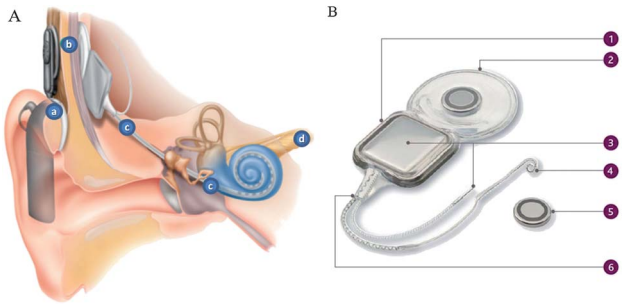

Fig. 1 Cochlear implant (Bionic Ear). Schematic of the internal components of the implant showing the electrode array sitting inside the cochlea (A): (a) the sound processor captures sound and converts it into digital code, (b) the sound processor transmits the digitally coded sound through the coil to the implant, (c) the implant converts the digitally coded sound to electrical impulses and sends them along the electrode array, which is positioned in the cochlea and (d) the implant's electrodes stimulate the cochlea's hearing nerve, which then sends the impulses to the brain where they are interpreted as sound. The CI512 implant showing the internal components of the Nucleus® 5 system (B): (1) receiver stimulator in titanium casing; (2) implant coil which enables telemetry; (3) two extracochlear electrodes; (4) precurved perimodiolar electrode array with 22 platinum electrodes (5) removable magnets for MRI safety and (6) symmetrical exit leads from casing. Previously published images are reproduced with permission. Reproduced with permission from www.bionicsinstitue.org.

functional neurons in the retina[31–33] or direct stimulation of the optic nerve.[34–36] In cases where these regions are functionally compromised, the neurons within the visual cortex of the central nervous system[37,38] provide another target of interest. Current strategies for restoring lost vision by electrical stimulation of visual neural pathways within the visual cortex involve more complex electrode configurations ranging from: a four-contact single cuff,[34] a relatively thrifty (up to 16 electrodes) multi-electrode array,[36] and "higher-order" silicon-based multi-electrode arrays (initially 81-electrode array)[39] for cortical stimulation.

Regenerative bionics is a term coined in recent years to describe the development of conduits that facilitate tissue regeneration (*e.g.* nerve or muscle) or connectors to prosthetics (*e.g.* neural driven prosthetics). The electrode–cellular interface remains the "Achilles heel" of regenerative bionic devices and will continue to determine overall performance. The composition and (nano) structure of the electrodes used in bionic devices are critical in that they determine the nature of the electrode–cellular interface that assembles in response to this foreign body (implant) invasion.

The nature of the interface in turn determines the ability to transport and transfer charge, ions or molecular species across it, which then dictates the level of communication attainable between the bionic device and the living system. Given the impact of nanostructure on the physical and chemical properties of materials, this will undoubtedly impact on their effectiveness in providing an appropriate electrode–cellular interface.

3. Electromaterials for bionics

Charge transfer at the electrode–electrolyte interface during cell stimulation may be either non-Faradaic or Faradaic in nature. Non-Faradaic processes involve a charging of the interface whereas Faradaic processes involve transfer of electrons and transformation of chemical species. Generally, non-Faradaic processes are preferred since no chemical species are created or consumed, providing safer stimulation as well as longer service life of the stimulation electrodes. Where Faradaic processes occur, the electrode must deliver appropriate charge without causing damage to the cells or inducing the formation of damaging products, or inducing corrosion processes that cause premature failure of the electrodes.[40] Tissue damage can be induced by the stimulation process if the excitable tissue is overstimulated or toxic electrochemical reaction products are created.[40,41]

Common strategies applied to avoid or minimize tissue damage include avoiding irreversible Faradaic reactions, applying charge-balanced stimulation waveforms and discharging the electrode after each pulse.[40,42,43]

While the use of metal electrodes predominates in existing medical bionic devices, the potential use of other electronic conductors (in particular carbons and organic conducting polymers) is uncovering new possibilities in the area of medical bionics. The presence of a conducting polymer coating on the metal electrode can greatly enhance the charge injection capacity. For example, a poly(ethylenedioxythiophene) (PEDOT) coated Pt film could deliver a charge injection limit of 2.3 mC cm^{-2}, about 10 to 20 times higher than the bare Pt film.[44] In addition, conducting polymer coatings can also improve the neural tissue–electrode interface by minimising the modulus mismatch and increasing the effective lifetime of these implants.[45] Similarly, carbon nanotube coatings on conventional tungsten and stainless steel wire electrodes could enhance both recording and electrical stimulation of neurons by decreasing the electrode impedance and increasing charge transfer.[46] A high injection limit of 1–1.6 mC cm^{-2} was reported for a carbon nanotube microelectrode array.[47]

Here we review the routes to nanostructured electrodes based on each of these classes of materials. This includes electrochemical depositions and treatments, structures obtained from processed nanodispersions and those obtained by nanofabrication. We then review studies to date that discuss the effect of nanostructure on electrode cellular. Finally, we briefly review progress in two areas that are critical to advances in Nanobionics, namely Nanofabrication and Nanobiocharacterisation.

3.1 Metal electrodes

Metallic electrodes that are biocompatible and corrosion-resistive include platinum, platinum–iridium alloys, gold, iridium, stainless steel, tungsten, titanium, titanium nitride, titanium dioxide and tantalum/tantalum pentoxide.[40,42,48] Nobel metals such as Pt, Ir and Au are non-reactive and corrosion-resistant. Other metals owe their corrosion resistance to the formation of a stable passive layer of metal oxide on the surface.[49] The most commonly employed metals and metal compounds for bionic devices are platinum, iridium oxide, titanium dioxide and titanium nitride.

A low impedance electrode–tissue interface is required to maintain signal quality for recording and effective charge transfer for stimulation. A decrease in electrode size with

a concomitant increase in electrode number is required to increase the effectiveness of recording and stimulation. Unfortunately, a decrease in size is often accompanied by an increase in impedance unless the effective electroactive area of the electrodes is increased by nanostructuring.

A smooth Pt electrode offered a capacitance of 20 μF cm^{-2} and high impedance of 557 MΩ $μm^2$ at 1 kHz frequency.[50] To increase the electrode surface area and decrease electrode impedance, a layer of 1D or 3D nanoporous Pt film has been electroplated with controlled structure and thickness.[51–53] Such nanoporous Pt electrodes possess an extremely large surface area. The 3D nanoporous Pt electrode electroplated from the reverse micelle phase could achieve a high charge injection limit of 3 mC cm^{-2} and low impedance of 0.039 Ω cm^2 at 1 kHz;[54] performance comparable to that obtained with iridium oxide. Amorphous iridium oxide was reported to possess much higher charge storage capacity and lower impedance in the high frequency range, 4.14 mC cm^{-2} and ~40–50 Ω, in sharp contrast to 0.2 mC cm^{-2} and 60–70 Ω for a crystalline IrO_2 film. After an electrochemical activation process of both amorphous and crystalline films, the charge injection capacity was significantly increased to 14.14 mC cm^{-2} and 1.6 mC cm^{-2}, respectively, due to an increase in surface area with roughness observed in the nanodomain.[55] Although titanium oxide is not yet a commonly used stimulation electrode, the anti-inflammatory and tunable electrochemical behaviour make it an attractive material for the fabrication of implantable devices.[56]

3.1.1 Fabrication of nanostructured metal films. Electrodeposition and sputter coating are two commonly used techniques to produce nanostructured metal or metal compound surface films on stimulation electrodes.

3.1.1.1 Electrodeposition. Electrochemical deposition is an effective and widely used technique in nanomaterials fabrication, wherein the structures produced are controlled by adjusting the electrochemical parameters.[57] Both direct electrodeposition and template-assisted electrodeposition are useful in this regard.

3.1.1.1.1 Direct electrodeposition. Activated iridium oxide films have been obtained by electrochemical deposition from an electrolyte containing the metal salt and using a symmetric potential pulsed profile.[58] The film obtained was composed of particles with a diameter of ~50 nm and exhibited a cathodic charge storage capacity of ~15 mC cm^{-2}. Particle diameters of ~10 nm have been attained by varying the electrolyte composition and electrochemical deposition parameters.[59] Nanostructured Pt black is often deposited onto Pt neural electrodes to increase the electrode surface and achieve a concomitant decrease in electrode impedance. The plating mixture consisted of hexachloroplatinic acid hydrate and monohexadecyl ether. The electrodeposition of nanostructured platinum film on Pt electrodes has been achieved either by constant potential[60] or by using voltammetric sweeps.[61] The Pt nanostructure obtained has a high charge capacitance (6 mF cm^{-2}, 1 kHz)[50] and a lower impedance (0.112 Ω $μm^2$, 1 kHz).[60] However, platinized Pt (Pt black) is rarely used for implants due to the lack of mechanical robustness in terms of abrasion resistance. It has been reported that electrodeposition under ultrasonication enhances the adherence and durability of Pt black produced on micro-wire based multi-electrode arrays.[62] Under sonication, only those Pt black particles that form strong bonds with the underlying substrate remain attached during the plating process.

TiO_2 nanotube arrays can be formed by anodising Ti foil in a methanesulphonic acid solution containing fluoride ions.[63] The formation of ordered and uniformly distributed nanotubes on the Ti surface was ascribed to the competing reaction between an electrochemical formation and a chemical dissolution of oxides. The nanotube dimensions could be controlled, with an inner diameter range of 20–100 nm, wall thickness of 10–20 nm and tube length from 200 to 500 nm. For example, TiO_2 nanotubes with a diameter of ~100 nm were prepared by anodising Ti foil in 0.5% aqueous hydrofluoric acid at 20 V for 40–60 minutes at room temperature. Smaller diameter nanotubes of ~50 nm and ~70 nm could be obtained at lower voltages of 10 and 15 V, respectively.[64]

3.1.1.1.2 Template-assisted electrodeposition. Well-defined 1D nanostructures including nanopillars, nanotubes or nanorods can be obtained by template-assisted electrodeposition. The resulting structures can be easily controlled by adjusting various parameters. Nanopillar-structures of TiO_2 with heights of 15, 55 or 100 nm could be produced on a Ti surface in 0.3 M oxalic acid using an anodization potential at 15, 40 or 70 V, respectively, through an alumina mask intermediate.[65] In this process a porous anodic alumina mask was formed by anodising the Al coating (~1 μm) on the Ti surface, and used as a template to pattern the Ti with self-arranged dot and pillar-like nanostructures. When aluminium is deposited and anodized on top of a Ti substrate, the Ti is subsequently anodized through the base of alumina pores with the nanosized pattern of the pores inherited on the substrate.

In addition, a combination of the direct and template-assisted electrodeposition methods is used to produce heterostructured metal–metal oxide materials (*e.g.* IrO_2/Au nanowire electrodes). Nanowire-structured Au was firstly produced by growing an Au film inside polycarbonate membrane pores at 0.65 V (*vs.* Ag/AgCl), followed by the electrodepostion of iridium oxide films by cyclic voltammetry.[66] This heterostructured material exhibited an enhanced charge capacity and decreased impedance compared with the Au nanowires of the same surface area.

3.1.1.2 Sputter coating. Sputter coating is another important and effective technique used in the fabrication of nanostructured films on electrode surfaces, particularly the fabrication of iridium oxide and titanium nitride by reactive sputtering.[67] Sputtered iridium oxide films (SIROFs) were deposited on microelectrode arrays by DC reactive sputtering from an iridium metal target. The thickness of the SIROFs produced ranged from 200 to 1300 nm. SIROF morphology with a thickness of 770 nm is comprised of densely packed nodules that are approximately circular with a diameter of 200–400 nm. It delivered a charge storage capacity (CSC) of 194 ± 2 mC cm^{-2} in phosphate-buffered saline (PBS).[68] The degradation of SIROF and activated iridium oxide films (AIROF) films on Utah electrode arrays (UEAs) was investigated during the charge injection consistent with functional electrical stimulation (FES).[69] The damage threshold for SIROF coated electrode tips was between: 60 nC

with a charge density of 1.9 mC cm^{-2} per phase, and 80 nC with a charge density of 1.0 mC cm^{-2} per phase. For AIROF coated electrode tips, the threshold was between: 40 nC with a charge density of 0.9 mC cm^{-2} per phase, and 50 nC with a charge density of 0.5 mC cm^{-2} per phase. The better stability of SIROF was attributed to the higher density of SIROF compared to AIROF.

Titanium nitride of columnar structure can be deposited by reactive sputtering of titanium in Ar/N_2 plasma.[70] The impedance for a 10 μm-diameter electrode could be reduced from a few MΩ to about 100 kΩ at 1000 Hz by increasing the active surface area. Rough, grain-like TiN coated electrodes showed an interfacial capacitance about 400 times higher than the smooth electrode due to its much higher surface area.[71] However, the interfacial region cannot be fully utilized due to the added resistance in the pores. For the sputter coated Pt electrode, an electrochemical platinum coating process was applied to achieve the high corrosion resistance and low impedance.[72]

3.2 Carbon electrodes

Limited forms of carbon nanotube structures can be obtained by a wide range of synthesis and fabrication techniques. Each technique facilitates the formation of unique nanostructured materials, possessing a wide range of physical properties. The challenge facing researchers in the field of medical bionics is choosing the appropriate fabrication method to produce the carbon based nanostructured materials that possess the appropriate physical properties to support and enhance cellular growth and proliferation. In addition, these nanostructured electrodes need to be able to electrically stimulate the adhered cells in a safe and efficient manner.

3.2.1 Direct growth. Chemical vapour deposition (CVD) can be used to create CNT structures in a structure suitable for nanobionic applications. A very elegant way to produce CNT electrodes is *via* the direct growth of horizontally or vertically aligned CNT arrays.[73] Typically, horizontal arrays are formed by direct growth of the CNT wires between controlled surface sites by catalyst patterning.[74] The large scale synthesis of vertically aligned CNTs was first reported by Xie *et al.*[75] In recent times many research groups[76–78] have produced vertically aligned CNT arrays using a variety of techniques. Novel aligned carbon nanotube electrode structures have been used to achieve charge storage in a Li-ion battery configuration, with a discharge capacity of 265 mA h g^{-1} reported.[79]

This performance pales into insignificance given the more recently reported discharge capacity of 546 mA h g^{-1} for a carbon nanoweb electrode produced by coating a carbon fiber paper.[80] Carbon nanowebs are produced using a CVD method with the conditions used being such that a wide range of substrates can be directly coated.[81] These nanoweb electrodes have proven to be resistant to protein fouling when tested in biologically relevant media.[82]

For the production of graphene films, CVD has emerged as the leading growth method that is inherently scalable for large area film production.[83] A second key advantage of using CVD based methods is the ability to dissolve the underlying metal for transferring graphene to an arbitrary substrate. To date, Ni[84] and Cu[85] are two common choices, among the metals used in CVD growth of graphene. Electrochemistry of the CVD produced graphene shows a 10 fold increase in electron transfer rates compared to bulk graphite.[86]

3.2.2 Carbon nanodispersions. The production of stable nano-carbon dispersions opens up a number of routes to electrode fabrication. Covalent or non-covalent attachment of functional molecules such as surfactants, synthetic polymers, or biomolecules has been employed to promote formation of stable nanodispersions.[87–90]

3.2.2.1 Carbon nanotubes

3.2.2.1.1 Covalent. Carbon nanotubes can undergo chemical functionalisation to enhance their solubility in various solvents. Covalent attachment of chemical groups, through reactions on the conjugated skeleton of CNTs, allows functional groups to be attached to tube ends or sidewalls. Chemical functionalisation of CNT tips has been performed mainly on the basis of oxidative treatments. As a general rule, CNT oxidation yields opened tubes with oxygen-containing functional groups (predominantly carboxylic acid) at both the sidewall and the tube endings. These groups can then be used as chemical anchors for further derivatisation. Although the bonding in CNTs is similar to that of graphene, curvature of the nanotube sidewall renders addition reactions to the cylindrical nanostructure more favourable than in a flat graphene sheet.[91]

3.2.2.1.2 Non-covalent. Surfactants. A variety of surfactants (including Triton X-100, sodium dodecylsulfate and sodium dodecylbenzenesulfonate) have been used to assist carbon nanotube dispersion in water. This widely used process involves high power sonication to break the CNT bundles. The hydrophobic component of the surfactant adsorbs onto the CNT surface with the polar component facilitating CNT stabilization in aqueous environments. Due to batch-to-batch variation of CNT production, many parameters in this procedure (including sonication duration and power, and nanotube-to-surfactant concentration ratios) require continued optimisation.

Synthetic polymers. Conjugated polymers can adsorb onto CNT surfaces by π–π interactions and have therefore have been used to modify CNT surfaces. Strong π–π interactions between CNTs and conjugated polymers, for example, poly(*m*-phenylene vinylene) (PmPV)[92,93] or poly(3-hexylthiophene) (P3HT),[94] drives the wrapping of the polymer around the CNT. The aqueous solubility of CNTs may also be improved by wrapping CNTs in water-soluble conjugated polymers, such as poly[*p*-{2,5-bis(3-propoxysulfonic acid sodium salt)}phenylene] ethynylene (PPES), which includes negatively charged groups. The solubility of such constructs in water was higher than that of sodium dodecylsulphonate (SDS)-wrapped CNTs.[95] Other polymers display weaker π–π interactions with CNTs, such as poly(vinyl pyrrolidone) (PVP), polystyrene-*block*-poly(acrylic acid) (PS-*b*-PAA),[96] or poly(styrene sulfonate), but these can also be used to wrap CNTs.[97]

Biopolymers. The use of biological molecules[98,99] as the dispersing agent has resulted in the formation of stable CNT dispersions. Molecules such as DNA,[100] chitosan,[100] gellan gum[101] and hyaluronic acid[98] have been used to great effect. Such stable dispersions have subsequently been used to fabricate nanostructured electrodes for use in photoluminescence,[102]

microbial sensors[103] and the fabrication of field-effect transistors.[104]

3.2.2.2 Graphene. It has long been known that graphite oxide (GO), a layered material that can be produced by controlled oxidation of graphite, can be well dispersed in water due to the presence of hydrophilic hydroxyl, epoxide, carbonyl and carboxyl functional groups. Ruoff and co-workers recently confirmed that GO can be fully exfoliated in water as individual graphene oxide sheets by sonication.[105] Although GO is electrically insulating, it can be conveniently converted back to conducting graphene *via* chemical reduction or thermal treatment.[105,106] Sonication of graphite in certain organic solvents, or in water in the presence of surfactants, can lead to partial exfoliation.[107–109]

Solution processability of graphene can be achieved through the reduction of GO. By simply adjusting the synthetic conditions, the resulting graphene can be readily dispersed in various solvents during the synthetic process, making it solution processable. Chemical conversion from GO leaves a small amount of residual oxygen-containing groups, which make the resulting graphene surfaces negatively charged and hence stabilised through electrostatic repulsion when dispersed in water.[106] Ruoff and co-workers have observed that stable dispersions can be obtained if the reduction of graphene oxide is conducted in certain organic solvents, such as *N*,*N*′-dimethylformamide.[110] Kaner and co-workers have found that graphene oxide can be dissolved in pure liquid hydrazine while being deoxygenated.[111] The resulting graphene can remain dispersed in hydrazine through the formation of a hydrazinium graphene complex in the absence of any surfactants.

The prevention of aggregation of graphene can also be realized by adding other stabilizing agents such as surfactants and polymers into the graphene oxide dispersion prior to deoxygenation.[112–114] This strategy enables functional molecules to be incorporated into graphene structures during processing to create novel nanostructured electrodes.

3.2.2.2.1 Surfactants. Surfactant-assisted exfoliation has been developed to disperse chemically unmodified graphene. Aqueous dispersions of relatively defect-free stabilized graphene can be prepared using ionic surfactants.[114–117] However, the reported concentrations were typically on the order of 0.01 mg mL^{-1}, which are too low for many practical uses.

3.2.2.2.2 Synthetic polymers. The use of polymer stabilizers rather than micelle-forming surfactants has shown promise in stabilizing dispersed graphene. In particular, Bourlinos *et al.* used polyvinylpyrrolidone (PVP) as a "coating" polymer to prevent graphene aggregation in aqueous dispersions.[118] This approach uses only sonication and avoids oxidation or other covalent functionalization.

3.2.3 Vacuum filtration. Vacuum filtration has been used to form free-standing electrodes comprised of a planar mat of entangled CNT (or more commonly known as "bucky paper") from CNT dispersions.[119,120] This method results in a robust, stand-alone material (up to several hundred μm thick) that can be easily peeled from the filter support. Apart from the obvious applicability as electrode materials for batteries and supercapacitors, this electrode configuration enables the study of the electromechanical actuation behaviour (expansion and contraction to do mechanical work) of CNTs upon application of appropriate potentials.[121]

This filtration process has also been used to form ultrastrong, smooth, and shiny graphene paper with a layered structure (Fig. 2A and B) by vacuum filtration of well-dispersed graphene dispersions.[106] Moderate thermal annealing further enhanced its mechanical properties and electrical conductivity. The as-formed graphene papers exhibit a combination of exceptional mechanical strength, thermal stability, high electrical conductivity and biocompatibility, making them a uniquely promising material for many technological applications.[122] Graphene hydrogel structures (Fig. 2C and D) can also be formed by the vacuum filtration of graphene dispersions.[123] Li and co-workers[123] found that if they prevented the graphene paper from drying out after filtration, it was possible to produce a hydrogel paper that contains approximately 92% water. Orientation of individual sheets results in exceptional electrical (0.58 S cm^{-2}) and mechanical properties (ultimate tensile stress is 1.1 ± 0.2 MPa). These values are the highest recorded values for conducting hydrogel structures.

In a further study we have shown that composite electrodes containing CNTs and graphene have superior electrochemical properties in terms of charge storage capabilities.[124] Our work showed that GO can serve as a superior dispersant to disperse pristine CNTs into water to form stable suspensions through supramolecular interactions. The hybridisation of GO with CNTs can promote the electrochemical conversion of GO to

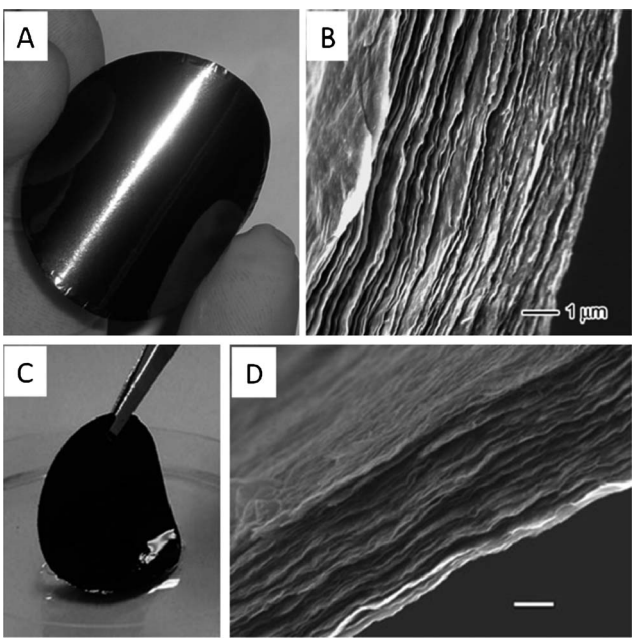

Fig. 2 Photograph of graphene paper prepared by vacuum filtration of a graphene dispersion (A) and SEM image of the cross-section of graphene paper showing a layered structure (B). Photograph of the as-formed graphene hydrogel film peeled off from the filter membrane (C) and SEM image of the cross-section of a freezedried graphene hydrogel film (D); scale bar: 1 μm. (Reproduced with permission from ref. 122 and 123.)

graphene. These discoveries offer a very simple, cost effective and environmentally friendly strategy to address the long-standing processability issue of CNTs. It also allows convenient integration of the 1D CNTs with the 2D graphene to form hierarchically structured carbon nanohybrids with enhanced performances.

3.2.4 Layer-by-layer assembly. Nanostructured carbon electrodes can be prepared by judicious assembly of appropriate nanodispersions. In addition to the filtration method nanostructured electrodes can be fabricated through the techniques of layer-by-layer (LBL) assembly. Self-assembly *via* the LBL approach is a simple and cheap deposition technique as compared to thin film deposition techniques of other chemical processes. At the same time, it is one of the most precise coating techniques, being capable of coating nanostructures with very homogeneous films of controllable thickness with atomic resolution. Su *et al.*[125] demonstrated a surfactant-free method to fabricate large-area single wall CNT film based transparent conductive (SWCNT-TC) electrodes with uniform properties (optical: transmittance of approximately 71.9% at 550 nm and electrical: approximately 34.9 Ω sq^{-1}) *via* the fusion of LBL deposition. More recently LBL has been used to fabricate graphene based electrodes as the plate-like structure and surface charge on the graphene sheets make them amenable to self-assembly. Multilayer graphene/Prussian blue electrodes have been fabricated by LBL assembly and used in the simultaneous electrochemical and surface plasmon resonance detection of hydrogen peroxide.[126] Graphene has been used as a conducting spacer in the LBL formation of electrochemically functionalized multilayered nanostructured electrodes.[127] Electrochemical studies of these electrodes demonstrated that the assembled nanostructures possess excellent electrochemical properties and electrocatalytic activity toward the oxidation of nicotinamide adenine dinucleotide (NADH) and could thus be used as electronic transducers for bioelectronic devices. The LBL approach has also been used to fabricate nanostructured sensor electrodes for the detection of glucose[128,129] and dopamine.[130,131]

3.2.5 Printing. Fabrication of graphene based devices has employed soft lithography (micro-contact printing),[132] which provides a method to produce micro-dimensional electrodes. To produce electrodes orders of magnitude smaller (in the nano-dimension), more sophisticated approaches are required such as nano-lithographic patterning,[133–135] and dip-pen nano-lithography (DPN).[136] These techniques have been employed to fabricate electrodes from graphene dispersions[137] or by patterning nano-features onto monolayer surfaces of graphene sheets.[138] Whilst the electrodes produced using the fabrication tools are nano-sized in one dimension (typically in the *Z* direction – perpendicular to the substrate), they tend be approach the micro-dimension in the horizontal plane. This is a consequence of the plate-like structure of graphene sheets.

3.2.6 Spinning fibres. A very powerful synthesis technique for fabricating polymer–CNT composite fibres is electrospinning.[139–141] It offers a possible way to simultaneously align CNTs along a single axis during processing, without compromising the structural integrity of the individual CNTs. The electrospun material also provides a very large accessible high surface area. This large active surface area is an attractive property in battery applications where the interaction of the electrolyte with the electrode material determines battery performance. Kim *et al.*[142] used electrospinning to fabricate carbon nanofibre-based electrodes that exhibited a large accessible surface area, high carbon purity (without binder), relatively high electrical conductivity, structural integrity, thin web morphology, a large reversible capacity (*ca.* 450 mA h g^{-1}), and a relatively linearly inclined voltage profile.

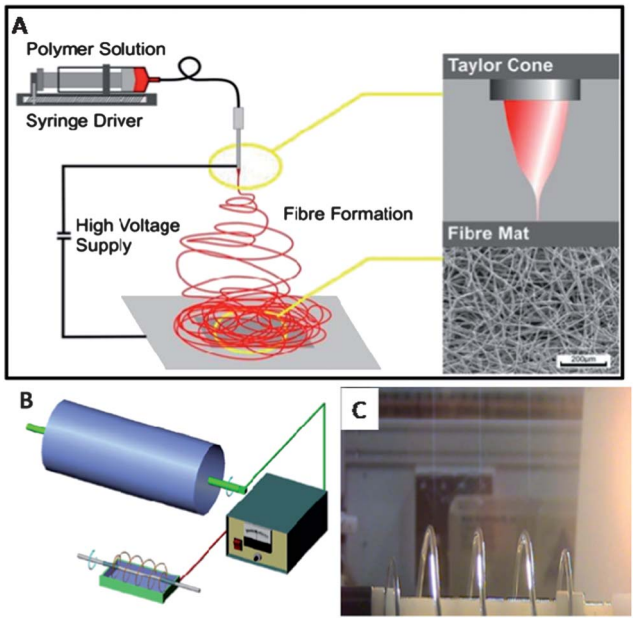

Fig. 3 (A) Schematic diagram of traditional electrospinning set up showing the Taylor cone and an SEM image of an electrospun mat. Schematic of novel needleless electrospinning design (B) and a photo of this system in operation (C).

Seoul *et al.*[143] showed for electrospun polymer–CNT fibres the percolation threshold for the insulator-to-conductor transition was 0.04 wt% CNTs for a CNT–PVDF electrospun fibre mat. They explained this low percolation threshold to be a consequence of the large aspect ratio of the CNTs used, resulting in entanglement of the CNTs at low concentrations. The incorporation of 20 wt% CNTs into polyacrylonitrile nanofibres resulted in a 144% increase in the nanofibre's tensile modulus (1.8 GPa at 0 wt% to 4.4 GPa at 20 wt%).[140]

Electrospinning has recently been used to form graphene containing nanostructured fibres. Zhu *et al.*[144] used electrospinning to incorporated graphene into a Li-ion battery anode in order to improve the electronic properties of spinel Li. The resulting nanosized architecture effectively shortens the distance for Li-ion and electron transport.

The materials fabricated from electrospinning are particularly attractive because their nanostructure mimics the three-dimensional random network of interconnected fibers and porous structures found in natural biological scaffolds such as the extracellular matrix, and thus is highly suited to biomaterial applications. More recent advances in the electrospinning design have seen the emergence of needle-less electrospinning[145] (Fig. 3B and C). This system uses a metal coil electrode rather than a single needle electrode resulting in large scale electrospinning.

Another approach to fabricate fibres using CNT as reinforcing additives is through wet spinning. Razal *et al.*[146] processed CNT dispersions into long lengths of fibre using a wet-spinning approach. The fibres produced were mechanically strong and possessed conductivities impressive for composite materials; in addition these fibres supported the growth of fibroblast cells with no apparent cytotoxic effects. In other unpublished work, a CNT–chitosan composite fibre containing the drug dexamethasone was produced, and controlled release under electrical stimulation was demonstrated. The production of micro-scaled drug delivery systems is appealing for biomedical applications where precise targeted delivery is required. More recently, we have incorporated chitosan and other biopolymers into wet-spun fibres comprising CNT to form composites, including chitosan–PAni–CNT fibres[147] and gel-like CNT–chitosan or CNT–gellan gum fibres.[148,149]

3.3 Organic conducting polymer (OCP) electrodes

The most practically useful (environmentally stable) and cytocompatible OCPs that have emerged from the past three decades of study are based on polypyrrole (PPy) and (PEDOT). It turns out that these dynamic materials have properties that provide a unique perspective on how the bionic interface might be controlled and developed.

OCPs provide two routes to nanostructured electrodes: electrodeposition as per metals, or formation of assemblies from nanodispersions as per nanostructured carbons.

3.3.1 Electrodeposition. Polypyrrole (PPy) can be formed by the oxidation of pyrrole at a suitable anode in an electrochemical cell to form an insoluble, conducting polymeric material as a deposit on the anode.

The dopant content in OCPs is high and can be greater than 50% w/w. The incorporation of an appropriate dopant forms a major constituent of the composition and hence the inherent chemical–biological properties. Chondroitin sulphate, dextran sulphate,[150] hyaluronic acid[151] or heparin[152] are readily incorporated into PPy during electrosynthesis.

Electropolymerization is most suitable for coating other conducting materials such as metals or carbon materials since the polymer produced is usually insoluble and deposits on these conductors in a manner akin to electroplating. The simplest means of inducing the polymerization process for PPy is to apply a sufficiently positive constant potential. The potential chosen will influence the rate of oxidation and, therefore, polymerization. An alternative is to apply a constant current to drive the reaction. This provides more accurate control over the rate of polymerization. The current density required for successful polymerization varies greatly depending on the dopant species to be incorporated with the monomer. For example, current densities as low as 0.25 mA cm^{-2} have been used to polymerize PPy with the biological dopant hyaluronic acid,[153] whilst polymerization of PPy with the dopant *para*-toluene sulfonic acid (*p*TS)[154] has been performed at 2.0 mA cm^{-2}. By varying electrodeposition parameters such as current density, working electrode properties, dopant type/concentration and electrolyte, the inherent 'cauliflower' nanostructure of OCP films can be controlled to exhibit very flat to highly rough surfaces. A well aligned cone-shape nanostructure of PPy is achieved by using simple, template free anodic electrodeposition.[155] Hydrogen bonding introduced from the use of a phosphate buffer solution as the electrolyte is proposed to promote the formation of the nanostructure, while steric hindrance from a high concentration of pyrrole monomer boosts the vertical growth and cone-shape formation.

Poly(3,4-ethylenedioxythiophene) (PEDOT) films form a flower-like nanostructure when electrochemically deposited on indium tin oxide (ITO) electrodes simply by one-step cyclic voltammetry (CV) in aqueous media without surfactant.[156] The flower-like hierarchical structure is composed of nanosheets with a thickness of even less than 2 nm at the edge, resulting in a highly porous structure. OCP nanowires,[157] nanobrushes[158] and other highly porous nanostructured electrodes[159] formed through both template (*e.g.* electrodeposited on an existing highly nanostructured electrode) and template free methods are achievable.

3.3.2 Nanodispersions. It is envisaged that nanodispersions will play an important role in enabling the fabrication of OCP electrodes in a range of different forms. For example, many of the current printing technologies such as ink-jet and extrusion printing are heavily reliant on the properties and compositions of inks containing nanoparticulates.

Conductive electroactive colloids of polypyrroles (PPy) or polyanilines (PAni) can be prepared by carrying out the oxidative polymerization in the presence of a steric stabilizer,[160] which physically adsorbs onto the growing polymer, preventing its aggregation and macroscopic precipitation. The process results in sub-micron OCP particles that are readily dispersed throughout other solutions for subsequent processing into composite structures. Stabilizers such as polyvinyl alcohol (PVA), polyvinyl pyrrolidone (PVP) and polyethylene oxide (PEO) have been used and OCP particles with sizes in the range 10–100 nm can be prepared.

Another approach to the formation of PPy and other OCP nanoparticles is the use of micellar polymerization and microemulsion techniques. The advantage of such an approach is that the particle size can be predefined by establishing the appropriate size and geometry of the templating micelle. Using this approach, Jang and co-workers[161] have reported the synthesis of PPy nanoparticles of 2.0 nm in size. PEDOT can also be polymerised from an aqueous environment using the micellar route. PEDOT nanoparticles with diameters in the range 35–100 mm have been prepared with conductivity of approximately 50 S cm^{-1}.[162]

Biological molecular templating is an alternative soft-template strategy that takes advantage of the exquisite structure and repeating charged groups/moieties on these biomolecules. DNA in particular is capable of directing chemical interactions in a stereo-selective manner to form chiral conducting polymer nanostructures. For example, both electrochemical and chemical polymerization of PAni, PPy and PEDOT on template DNA has successfully resulted in the fabrication of nanowires and structures related to the chiral nematic liquid crystallinity of DNA.[163–165]

Chitosan has been used as a molecular template to promote formation of nanosized PPy particles on silica.[166] Interestingly, another biomolecule (heparin) has been shown to have a similar templating effect. In the case of heparin, it acts as both the

molecular dopant and a (nano) structure directing template.[167] Others[168] have used lipid tubules as templates during chemical oxidation of pyrrole to form nanofibers with diameters between 10 and 50 nm and lengths reaching up to several hundred microns.

3.3.3 Printing OCPs. A commercial PPy dispersion from Sigma Aldrich (Product number 482552) was modified by addition of ethylene glycol (10%) to reduce viscosity to less than 100 mPa s and obtain a surface tension of approximately 35 mN m^{-1}, and hence produce an ink-jet printable formulation.[169] These formulations were printed into chemical sensors that demonstrated relatively high sensitivities for inkjet-printed PPy thin films to alcohol vapours. The work described presents favourable results for the concept of using of inkjet printing as a simple means of producing chemiresistor sensors based on OCPs. The OCP PEDOT:PSS produced in the form of dispersions has also been printed using inkjet technology and used for the detection of organic vapours.[170]

A route for generating arrays of printable poly-3-alkylthiophene-based gas sensor materials suitable for low-cost manufacturing has been reported.[171] Materials with complementary sensor responses were synthesized by incorporating functional groups into the thiophene molecule, either along the polymer backbone or as end-capping groups. Using these materials as printable sensor inks, a functional, integrated gas sensor array chip was fabricated using additive deposition techniques. The sensor array showed sensitivity to a range of volatile organic compounds down to concentrations of 10 ppm. Biosensors have also been fabricated by inkjet printing of PEDOT:PSS and glucose oxidase (GOx) onto ITO glass[172] (Fig. 4). The printed structures were encapsulated with a cellulose acetate membrane to prevent dissolution of the active layers.

The versatility of printing has seen the emergence of bioprinting based on inkjet and related printing technologies, which can be utilised to fabricate persistent biomimetic patterns that can be used both to study the underlying biology of tissue regeneration and potentially be translated into effective clinical therapies.[173]

3.3.4 Spinning fibres. There has also been much interest in the formation of OCP nano-fibres using the electrospinning technique (Fig. 5).[174–176] It is possible to electrospin fibres from soluble PPy solutions. For example, electrospinning has been used to produce 3 μm diameter PPy/dodecylbenzene sulfonic acid (DBSA) fibres collectively in the form of a non-woven mat that, following compression, gave conductivities of ≈0.5 S cm^{-1} (*e.g.* slightly higher than those of powder or cast films).[177] An alternative is to first electrospin the fibres from a chemical oxidant/polymer mixed solution followed by exposure of the fibres to pyrrole vapour.[178] This approach has produced PPy/poly(styrene-β-isobutylene-β-styrene) (SIBS) nanofibers capable of aligning neurite outgrowth.[179]

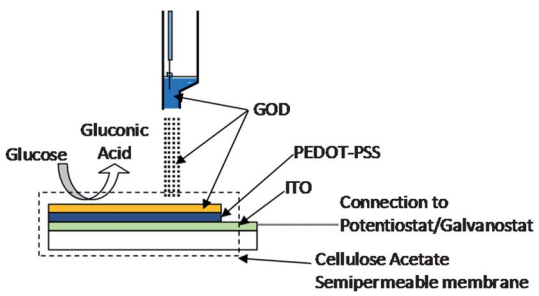

Fig. 4 Diagram of the prototype of the complete GOx inkjet printed electrode.

The electrospinning of polythiophenes, particularly poly-3-alkylthiophenes has been previously reported by many researchers.[180–185] The properties of electrospun PEDOT fibres have been assessed by changing the solvents and their concentrations.[186] For example, when using butanol or 1-propanol as a solvent and poly(vinyl pyrrolidone) (PVP) as a matrix polymer, the electrical conductivity of PEDOT non-woven fibre mats was as high as 7.5 S cm^{-1}. Numerous other routes to incorporating a conductive PEDOT coating onto the electrospun fibres (*e.g.* biodegradable polymers and PAni) include the use of subsequent deposition of PEDOT *via* vapour phase deposition,[187] electrochemical deposition[188] and dip coating.[189] The highest conductivity value (60 S cm^{-1}) claimed for polymer nanofibres to date is for PEDOT fibres produced *via* an electrospun oxidant and vapour phase polymerization. Their high conductivities were attributed to a high degree of ordering of the fibres at the molecular level.

Polyaniline doped with camphorsulfonic acid and blended with poly(L-lactide-*co*-ε-caprolactone) has been electrospun to form conducting nanofiber cell scaffolds (Fig. 5) with individual fiber dimensions of approx. 400 nm and electrical conductivities of 0.0015–0.014 S cm^{-1}.[190] The scaffolds were used to investigate the effect of electrical stimulation on mitochondria metabolic activity for NIH-3T3 fibroblasts.

4. Electrode–cellular interaction: effect of nanostructure

The effect of nanostructure on cellular interactions with each of the three types of conductors of interest here: metals, carbons and organic conducting polymers, are explored below.

4.1 Metals

It is reported that human mesenchymal stem cell (hMSC) growth on TiO_2 nanotubes was determined solely by geometric cues on the surface.[191] On small-diameter nanotubes cell adhesion was increased but growth occurred with minimal differentiation; behaviour attributed to the protein aggregate adhesion configurations induced by the small nanotubes. On large-diameter nanotubes, hMSC are forced to elongate and stretch to search for protein aggregates and, as a result, are forced/guided to differentiate specially into osteoblast cells. The effect of the height of titania nano-pillars on hMSC growth was investigated by Sjöström *et al.*[65] Osteoid matrix nodules containing osteocalcin and osteopontin were observed on pillar-like surfaces after 21 days culture, compared to very low levels of osteopontin and negligible osteocalcin presented on planar control surface. The occurrence of osteopontin- and osteocalcin-rich bone matrix nodules decreased as structures increased in height from 15 to 55 to 100 nm. It is also reported that the number of adhered

osteoblast cells on the TiO_2 nanotubes increased significantly (by ~300 to 400%) as compared to cells adhering to the Ti metal surface.[192] The explanation given was that the pronounced topological features significantly increased the surface area and possibly also the pathways for fluid between the nanotubes. On a nanosized TiN film with roughness ranging from 1.3 (grain size 21 nm) to 5.6 nm (grain size 41 nm), primary hippocampal neurons presented more preferential neuronal network morphology on those with lower roughness values and decreased size of topographical features.[193]

Fibrous tissue growth around stimulation/recording electrodes after implantation can limit performance. It has been shown that surface nanotopography modulates the response of fibroblasts and glial cells to Pt surfaces.[194] Both fibroblasts and glial cells on smooth Pt surfaces developed peripheral lamellipodia, and an extensive network of actin filaments, to form characteristic stellate shape morphology (Fig. 6). In contrast, cells on the nanostructured rough Pt were more elongated with a lower prevalence of actin network formation (Fig. 6). An increase in both nanoscale roughness and height of the nanofeatures was related to a decrease in the proliferation of fibroblasts.[194] It was also reported that the number of fibroblasts growing on a Pt surface could be significantly reduced by increasing the height of individual whisker-like surface features.[195] A maximum difference in cell number of 187% was observed between the tallest surface features (39 ± 9 nm, 44 ± 5 cells mm^{-2}) and flat surface (6.3 ± 1.2 nm, 125 ± 6 cells mm^{-2}).[195] The reduced number of focal adhesion points might be the main contributor to the inhibition of the fibroblast growth on the nanostructured surface.

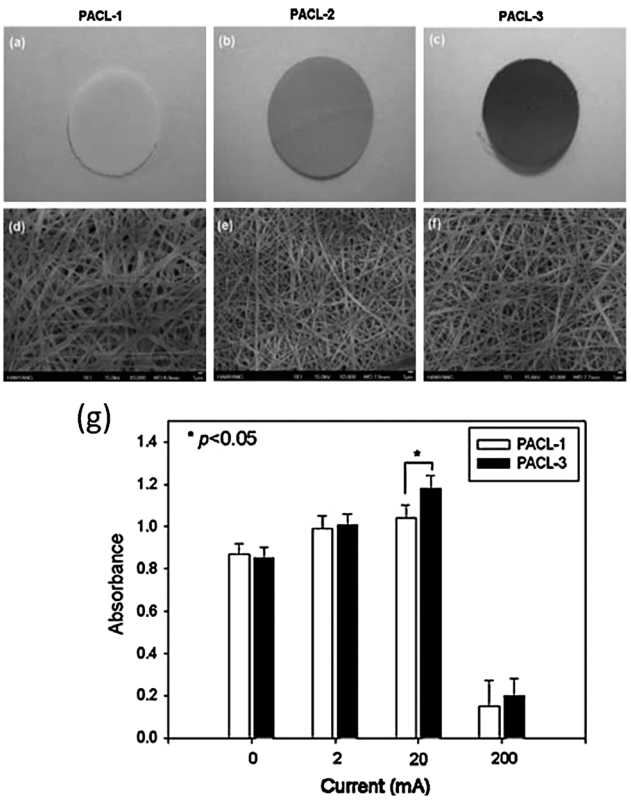

Fig. 5 Morphologies and fiber diameters of CPSA-PAni/PLCL nanofiber scaffolds. (a–c) Macroscopics, (d–f) SEM micrographs (g) mitochondria metabolic activity of NIH-3T3 fibroblast. (Reproduced with permission from ref. 190.)

4.2 Carbons

Carbon is an ideal biomaterial and has been used in the form of highly oriented pyrolytic graphite (HOPG) and composites containing carbon fibres.[196] These groups of "medically relevant" carbons elicit negligible (if any) adverse reaction in the host tissue and, additionally, are relatively unaffected by the host tissue environment into which they are introduced.[197] An attractive feature of carbon is that it can be synthesised and fabricated into numerous nanostructured formats such as nanotubes[198,199] and nanofibres.[200]

Nanostructure plays a critical role in modulating cellular interactions, and a number of studies have shown variations in cell adhesion in response to nanotopographical features.[201,202] Although cell responses vary between cell types and nanosubstrates,[203] the commonly observed trend is that substrates with nanotopographical features enhance cell adhesion. For example, Wan *et al.* found that osteoblast adhesion on both textured surfaces of microscale (2.2 μm) and nanoscale (450 nm) pits was increased compared with that on the smooth-surface

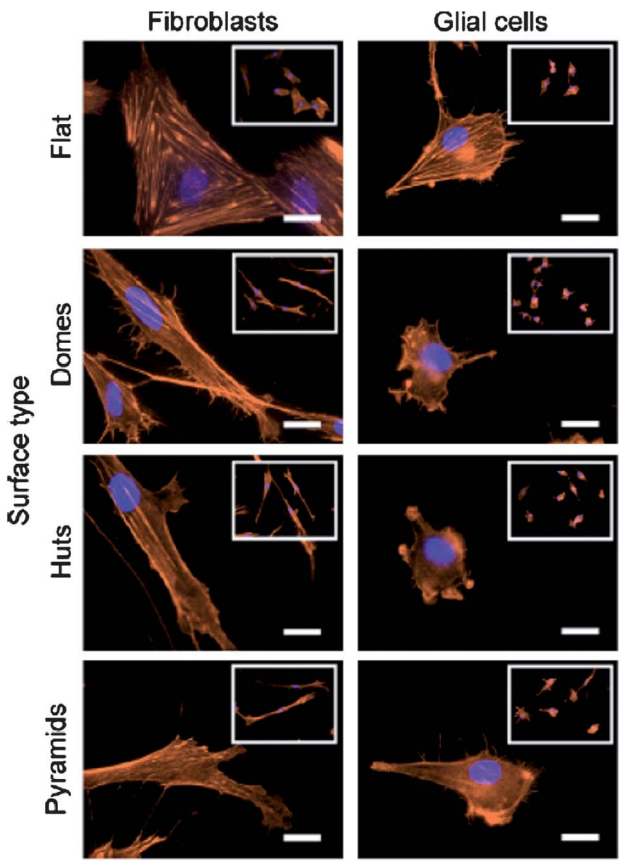

Fig. 6 Analysis of actin cytoskeleton on cells cultured for 1 day on the test surfaces. The images are representative of fibroblasts (first column) and glial cells (second column) cultured on flat surfaces and rough surfaces type of domes, huts and pyramids. The insets are images from the same cells taken at lower magnification, which show the general morphology of the cells on the surface. Scale bar = 15 μm. (Reproduced with permission from ref. 194.)

control, and that adhesion on the nanopitted surface was superior to the micropitted surface.[204] It should be noted that this observed trend is the opposite of what has been observed and discussed above for nanostructured Pt.

The feasibility of MWNTs to support neuronal growth was first investigated by Mattson *et al.*[205] The interactions of neurons with unmodified MWNTs and MWNTs functionalised with 4-hydroxynaneal suggest the suitability of MWNTs to support cellular growth. This property was further investigated by Hu *et al.*,[206] who studied the interaction of hippocampal neuronal cultures with functionalised MWNTs. Functionalisation was used to induce either a negative (MWNT–COOH), neutral (MWNT–PABS) or positive charge (MWNT–EN) on the MWNTs. The results showed that the outgrowth and branching patterns of the neural processes can be manipulated by varying the MWNT charge (Fig. 7). In general, as the MWNT charge went from negative through neutral to positive an increase in growth cones, longer average neurite length, and elaborate neurite branching was observed.

Correa-Duarte *et al.*[207] fabricated 3D networks as scaffolds for cell seeding and growth by functionalising aligned multi-wall CNT (MWNT) arrays to form unique 3D assemblies (Fig. 8). These researchers investigated the effect of this 3D structure on connective tissue cells using a common mouse fibroblast cell line (L929) and found these structures to be highly biocompatible and able to stimulate robust tissue formation.

Nguyen-Vu *et al.*[208] prepared a multi-composite CNT 3D structure by applying a thin layer of type IV collagen adsorbed onto vertically aligned MWNT to promote the adhesion of PC12 nerve cells. Post-adsorption of nerve growth factor (NGF) was additionally carried out to induce neurite outgrowth. In addition, electrochemical addition of a PPy coating had the advantage of: (1) preventing the collapse of the CNT structure, (2) improving the mechanical contact with cells and (3) decreasing the electrode impedance (Fig. 9).

These types of studies have paved the way for advances in interfacing CNT with cells and tissue particularly for neurophysiology applications.[209,210] For example, the use of CNT has significantly enhanced signal acquisition during *in vitro* and *in vivo* neural stimulation and recording in microelectrode arrays[47] and implantable electrodes.[46]

Carbon vapour deposited CNTs containing carboxyl derivatives have been used to provide a covalent anchor for NGF or brain-derived neurotrophic factor (BDNF) *via* carbodiimide chemistry.[211] In contrast to previous work on fixed CNT composite film structures, these CNT–NGF composites were endogenously introduced into the culture medium of embryonic dorsal root ganglion (DRG) neurons and were shown to induce differentiation. Implementing CNT composites with growth factors in this way is intriguing, particularly if some advantage could be gained from their conductive properties. However, further work is required to clarify the cell uptake of these CNT composites and its presently conflicting consequences.

Electrical signals are critical physiological stimuli that control the adhesion and differentiation of certain cell types.[212] Recent studies demonstrated the usefulness of carbon nanotubes blended with conductive polymers, *e.g.* polypyrrole (PPy), polythiophene (PT), polyaniline (PAni), for electrically conductive tissue engineering scaffolds.[213–215] A wide range of cells from amoebae to neurons have been shown to orient in electric fields, although the direction of orientation is dependent on cell type.[216] The prospect of using nanostructured electromaterials that incorporate stimulatory cues, such as electrical signals, to regulate cell attachment, proliferation, and differentiation[217] is an

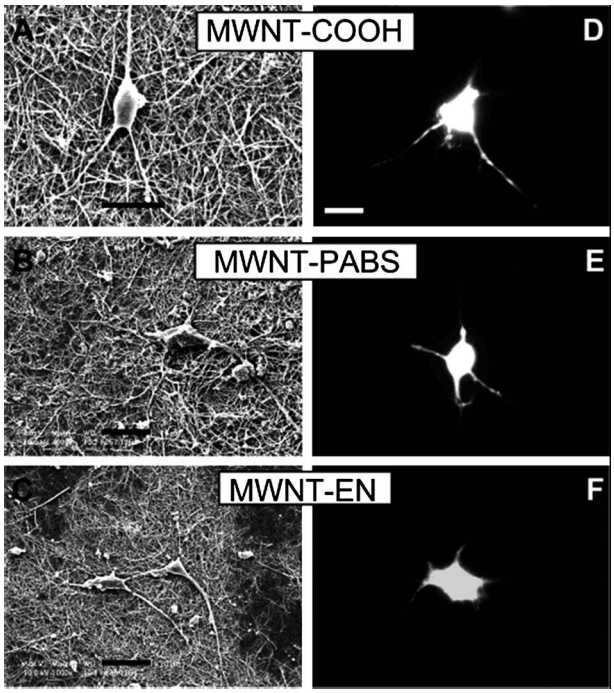

Fig. 7 Chemically functionalized MWNTs provide permissive substrates for neurons. (A–C) SEM images of neurons growing on different chemically functionalized MWNTs. (D–F) Fluorescent images of live neurons, accumulating calcein, which grow on different chemically functionalized MWNTs. Scale bar: 20 μm, except 10 μm in (A)–(B). Reproduced with permission from ref. 206.

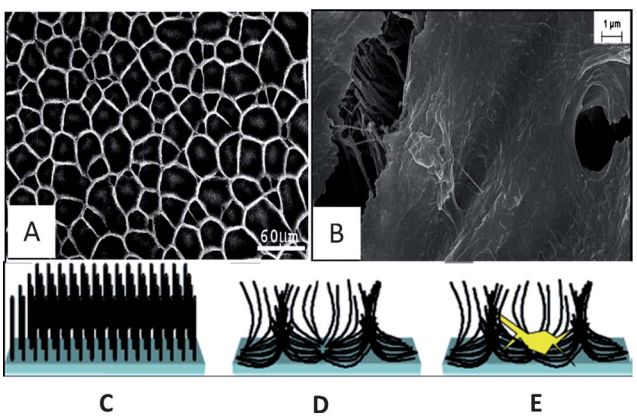

Fig. 8 SEM of (A) 3D networks of 50 mm length carbon nanotubes and of (B) L929 mouse fibroblasts growing on MWCNT-based network after 7 days. (C–E) Representation of the general method used to fabricate 3D MWCNT-based network and its application as a scaffold for cell growth. (C) MWNTs perpendicularly aligned to the substrate. (D) The latter were chemically treated to obtain a cross-linked 3D structure. (E) The 3D network, like a scaffold, favours cell growth. Reproduced with permission from ref. 207.

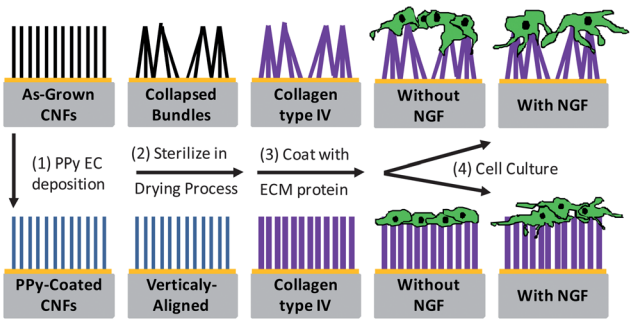

Fig. 9 Schematic of sample preparation for vertically aligned CNT–PPy–collagen–NGF composites. (Reproduced with permission from ref. 208.)

appealing one. It is to this end that CNTs are being studied as suitable platforms to support and interact with a variety of cell types.

Supronowicz and co-workers[215] incorporated CNTs within the traditional cell culture polymer polylactic acid (PLA) to fabricate a novel current-conducting composite for exposing osteoblasts to alternating current stimulation. Non-functionalised MWNTs were added to emulsions of PLA in chloroform and sonicated to ensure thorough mixing, followed by air drying to evaporate the chloroform away to leave a solid PLA–MWNT composite. These early studies clearly indicated the significance of electrical stimulation (10 μA at 10 Hz) on cellular responses, with a 46% increase in cell proliferation after 2 days, a 307% increase in the concentration of extracellular calcium after 21 days, and upregulation of mRNA expression for collagen type-I after both 1 and 21 consecutive days. More recently Shao *et al.*[218] produced conductive nanofiber meshes that offer a unique system for studying the synergistic effect of topographic cues and electrical stimulation on osteoblast outgrowth. The results of unstimulated obsteoblast assays showed that the aligned nanofibers, acting as topographic cues, could enhance the extension and direct the outgrowth of obsteoblasts better than random fibres. In the presence of a direct current (DC) of 100 μA, the obsteoblasts on all samples aligned with the direction of the flow of electrical current.

Graphene (G) and graphene oxide (GO) have recently attracted attention for potential use as cell culture substrates.[219] More recently, graphene has been used as a substrate to culture stem cells. For example, Nayak *et al.*[220] reported that graphene provides a promising biocompatible scaffold that does not hamper the proliferation of hMSCs and accelerates their specific differentiation into bone cells even in the absence of commonly used additional growth factors such as BMP-2. Induced pluripotent stem cells (iPSCs) have been cultured on G and GO. Chen

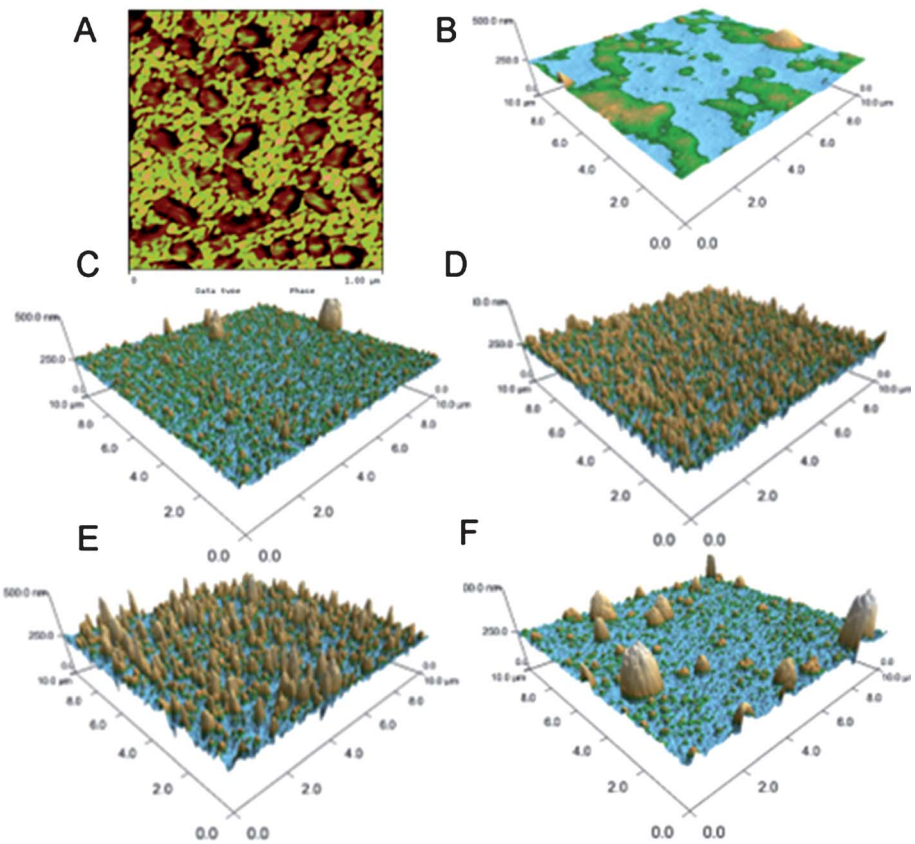

Fig. 10 (A) 1 μm micron AFM phase image of an electrochemically polymerized polybithiophene film. The changes in dark and bright contrast reflect variations in the polymer crystallinity (*e.g.* due to crystalline and amorphous regions). (B–F) AFM 3-D topographic 10 micron images of PPy films in order of surface roughness and their ability to support muscle fibre formation – (B) PPy/PMAS, (C) PPy/CS, (D) PPy/DS, (E) PPy/HA and (F) PPy/*p*TS. (Reproduced with permission from ref. 236 and 237.)

et al.[221] showed that iPSCs cultured on both G and GO surfaces spontaneously differentiated into ectodermal and mesodermal lineages without significant disparity, but G suppressed the iPSCs differentiation towards the endodermal lineage whereas GO augmented the endodermal differentiation. Human neural stem cells (hNSCs) have been cultured on G and demonstrated enhanced neuronal differentiation compared to a glass substrate control.[222] The G worked as an excellent cell-adhesion layer during the long-term differentiation process and induced the differentiation of hNSCs more toward neurons than glial cells. In addition, Park *et al.*[222] also found that G had a good electrical coupling with the differentiated neurons for electrical stimulation. These previous works collectively demonstrate that the surface properties of G governed stem cell behaviour and implicate the potential of G-based materials as a platform for stem cell culture with diverse applications.

4.3 Organic conducting polymers (OCPs)

Cellular interactions have been extensively explored using polypyrrole (PPy) or poly(3,4-ethylenedioxythiophene) (PEDOT). PPy has demonstrated cytocompatibility with various cell types including neurons and neuron-like cells,[223,224] endothelial cells,[225,226] muscle cells,[151] keratinocytes,[227] cardiac cells,[228] and mesenchymal,[229] embryonic and neural stem cells.[230] To date, *in vivo* tests of implanted PPy have shown that PPy is compatible with hypodermis tissues, brain tissue and peripheral nerve.[231–233] Similar to PPy, PEDOT has been used extensively for compatibility and neural recording/stimulation studies both *in vitro* and *in vivo*, particularly for neural tissue and neuronal cell lines.[234,268,269]

Given the ability to manipulate OCPs into various forms of nanostructures and nanopatterns, their interactions can occur at the same level as the molecular 'dashboard' of cells and therefore they are likely to have a profound effect on modulating cellular responses. The effect of controllable nanostructures and related nanoscale spatial variation in surface chemistry (*e.g.* hydrophobicity) on cellular interactions is already well-stated for many different types of biomaterials and their use in regenerative medicine.[235]

The inherent nanostructure of OCPs is dominated by close-packed nodular grains of nanoscale diameters, giving rise to the well-known 'cauliflower' structure. There is a strong correlation between this nodular surface morphology and the surface potential of the polymer.[270] It is believed that the nodules comprise dopant-rich, high conductivity regions where nuclei initially form and, subsequently, around which polymer preferentially grows. This nanoscale spatial variation in the surface potential and/or conductivity at the surface of the OCP films also correlates with nanoscale phase separations in the polymer crystallinity or Young's modulus[236] (Fig. 10A). It appears that many of these nanoscale variations in the surface properties are inextricably linked to the inherent polymer nanostructure, which is controllable through modulation of the electropolymerization deposition parameters and/or external electrical stimulation (*i.e.* redox switching). Their importance may manifest in fluid and biological environments and have an influence on bio-interactions (*e.g.* electrostatic binding) in the adhesion of proteins and cells.

For cellular interactions, the nanostructure has an effect on the ability of cells to firstly attach, and then proceed with normal cell differentiation. For example, AFM imaging reveals that the incorporation of *para*-toluene sulfonate (*p*TS) and PMAS, and other biological polyelectrolytes such as hyaluronic acid (HA), chondroitin sulfate (CS), dextran sulfate (DS), as dopants in PPy films has a dramatic effect on the surface roughness of their nodular morphologies[150,237] (Fig. 10B–F). While all these substrates support cell adhesion and proliferation to varying degrees, the capacity for muscle fibre formation is generally dependent on an increase in cell adhesion to the polymers, which correlates with a low surface roughness value of the polymers.[150] The existence of nanoscale topographic contributions to the presence of nucleation centres,[238] or changes in surface hydrophobicity of PAni films[239] have recently been suggested to promote the attachment and proliferation of PC-12 cells on PAni films.

Compared to the inherent nano-topography of electropolymerized OCP films, the nanostructure of OCP films acquired from the deposition of discrete nanomaterials such as electrospun nanofibres, and/or CNTs subsequently coated with PEDOT and PPy, can dramatically improve the growth of neural cells.[240] In experiments with primary neurons, DRG explants cultured on OCP nanotubes remained more intact and exhibited longer neurites compared to their film counterparts.[240]

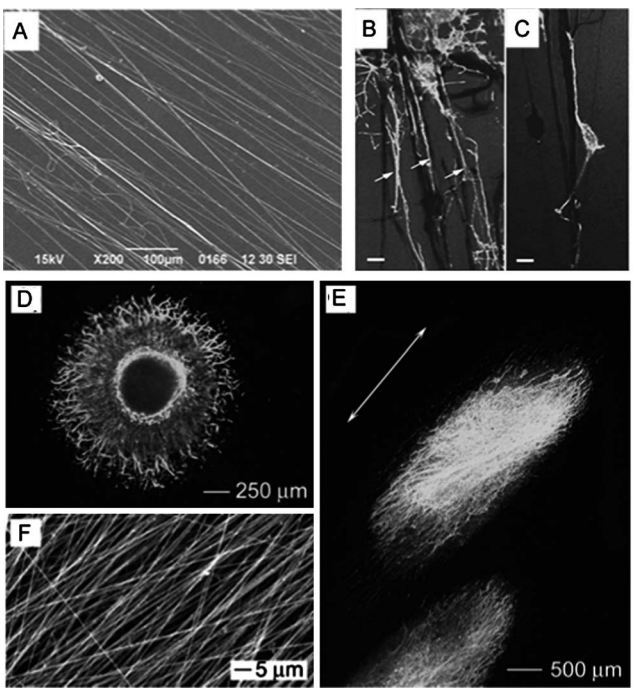

Fig. 11 (A) SEM images of aligned PPy–SIBS composite fibres. (B and C) Fluorescence micrograph showing aligned neurites of nerve cells (arrows) on the fibres (dark lines). Scale represents 10 μm. (D) Fluorescence micrograph showing the DRG neurite field on random PCL–PPy core–sheath nanofibers. (F) Aligned PCL–PPy core–sheath nanofibers. (E) Fluorescence micrograph showing the DRG neurite field on aligned PCL–PPy core–sheath nanofibers. (The arrow indicates the alignment direction for the underlying nanofibers.) (Reproduced with permission from ref. 179 and 242.)

Electrospun functionalized polythiophene fibres in the form of nonwoven mats or aligned mats, facilitated by a rotating collector drum, support the growth and differentiation of muscle cells.[241] Furthermore, the aligned fibres provide suitable 3D structures for guiding the alignment of developing muscle fibres. Electrospun, aligned PPy/poly(styrene-β-isobutylene-β-styrene) (SIBS) fibres significantly induce the parallel alignment of neurite outgrowths which can extend for ≈100–150 μm either alongside or directly on top of these nanodomain features (Fig. 11A–C).[179] Single neurites extending, and making contact, along a single fibre for 50–60 μm indicate that alignment is due to a contact guidance effect of the fibre, rather than the physical constraints of the parallel arrangement of the fibres. Conductive core sheath nanofibers prepared by *in situ* PPy polymerization of electrospun poly(ε-caprolactone) (PCL) and poly(L-lactide) (PLA) fibers similarly orient and dramatically enhance neurite growth (up to 87%) in terms of maximum length when uniaxially aligned conductive core–sheath nanofibers are compared with their random counterparts (Fig. 11D–F), and this was further increased through electrical stimulation.[242]

5. New trends in nanofabrication

5.1 Dip pen nanolithography of nano-electromaterials

Dip Pen Nanolithography (DPN) is a nanofabrication technique introduced by Mirkin and co-workers[243] that enables rapid manufacturing of devices requiring nanoscale structures and patterns. By using top down or bottom up approaches, the possibility to precisely place biomolecules and chemical gradients onto conductive and flexible substrates using DPN represents a high degree of control and resolution for device fabrication. Patterning of micro- and nano-circuits based on the deposition of conducting nanomaterials can also be achieved, which is critical for the varying structural dimensions of electronic components in bionic devices.

DPN operates by using existing Atomic Force Microscopy (AFM) technology to deposit a wide variety of chemicals and materials onto a surface *via* a sharp probe tip that acts like an "ink pen".[244] The conventional DPN approach, or "meniscus" method, involves the transfer of ink molecules to the substrate through a water meniscus bridging the tip and substrate (Fig. 12A). This method usually requires fine tuning of the substrate chemistry (*e.g.* functionalization with a charged monolayer or other coatings) to enable specific interactions between the ink and substrate that facilitate transfer and stable adhesion of the ink. In contrast, the "physioadsorption" method uses a carrier solvent to assist transport of the ink molecules and together they deposit onto the substrate *via* physioadsorption processes (Fig. 12B). This method compromises on pattern resolution, though it is more flexible and requires less sample preparation.

It is possible to directly deposit gold nanoparticles onto surfaces by immersing the DPN tip in a gold nanoparticle dispersion.[245,246] A dried coating of nanoparticles, which can be chemically functionalized prior to deposition to assist in surface recognition, is then able to freely diffuse through the tip-surface water meniscus. A solvent carrier can also facilitate the deposition of nanoparticles, as shown in Fig. 12B for a silver nanoparticle-solvent ink,[247] with subsequent curing at high temperatures used to evaporate the solvent carrier and form pure metallic patterns. Alternatively, the deposition of metals based on metallic ion 'inks' such as $HAuCl_4$ aqueous solutions can proceed *via* surface-induced reduction of Au(III) precursors to the insoluble Au(0) to form metallic gold nanostructures.[248] 100 nm block copolymer micelles have recently been used as 'carriers' of the metal ions to enable the formation of sub-10 nm gold particles during the reduction process[249] (Fig. 13). The block copolymer micelles highly localize the metal ions and dramatically lower the amount of metal ion in each patterned gold nanostructure compared to that made from pure metal ion inks. Similar template-assisted inks involve the use of metal nanoparticle-modified enzymes that act as a nano-templating agent for the growth of gold or silver nanowires.[250] These approaches provide a new paradigm for DPN patterning as the diverse array of micelle structures and enzymes available enables flexibility in the nanofabrication process. These and other types of DPN approaches are able to pattern a range of metallic, semiconductor and metal oxide nanostructures on surfaces.[251]

More recently, DPN has been used to fabricate CNT electrode structures. Duan *et al.*[252] used a conductive AFM tip to oxidize a silicon surface electrochemically, upon which single-walled CNTs were welded with a silicon oxide nanojunction. More specifically, Lee *et al.*[253] created nanojunctions between CNTs and metal electrodes by field evaporation of metals from an AFM tip coated with metal precursors to solder the nanotubes on the electrodes. The advantage of this technique is that the site of the nanojunction (soldering points) could be located specifically by engaging the AFM tip.

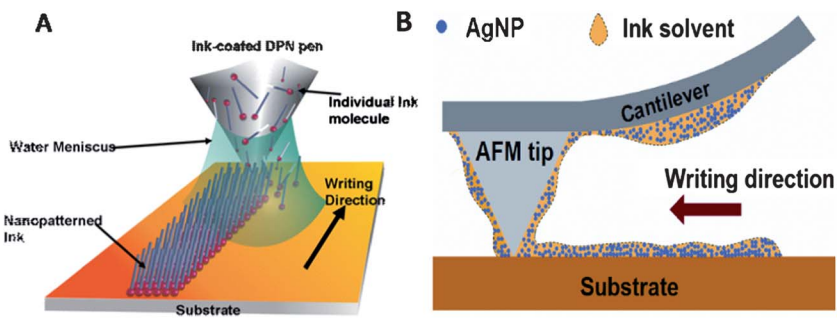

Fig. 12 Schematic of DPN mechanisms for depositing molecules *via* the meniscus method (A) and physioadsorption method (B). (Reproduced with permission from Nanoink Inc. and ref. 247.)

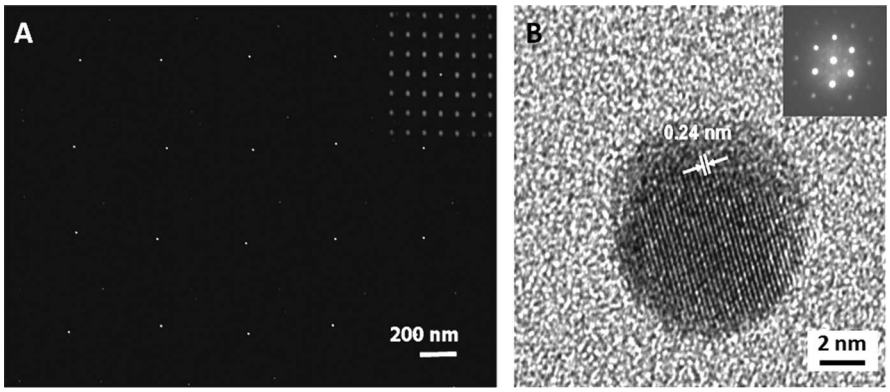

Fig. 13 (A) SEM image of sub-10 nm Au nanoparticles produced by plasma treatment. (Inset) Fourier transform of the SEM image. (B) High-resolution TEM image showing a crystalline Au nanoparticle with a diameter of 8 nm. The measured interplanar spacing of the crystal is 0.24 nm. (Inset) typical electron diffraction pattern of the synthesized Au (111) nanoparticle. (Reproduced with permission from ref. 249.)

Wang *et al.*[254] applied DPN toward patterning electrical contacts for nanoelectronic device fabrication. The advantages of such an approach include selective placement and design of electrical contacts, targeted device fabrication (*versus* random selection, as in electron-beam lithography of predefined contacts), minimal damage during the fabrication process (no electron irradiation), and the ability to image SWNTs and pattern contacts in one system under ambient conditions. This straightforward device fabrication technique allows for electrical measurements on SWNTs with various dimensions and chiralities.

Lu and co-workers[255] have used DPN to pattern OCPs by "writing" lines of a commercial PEDOT:PSS ink and demonstrated their use as nitric oxide gas sensors. Soluble self-doped sulfonated PAni (SPAni) and PPy have been patterned with 130 nm line widths onto chemically functionalized substrates to facilitate binding of the ink molecules.[256] DPN has also been used in a manner where the ink is comprised of monomer/oxidant constituents and the OCP is written as chemical polymerization occurs *in situ* beneath the probe tip.[257] Electrochemical-DPN is another interesting approach that relies on applying a voltage to the probe tip to electrochemically polymerize the polymer during

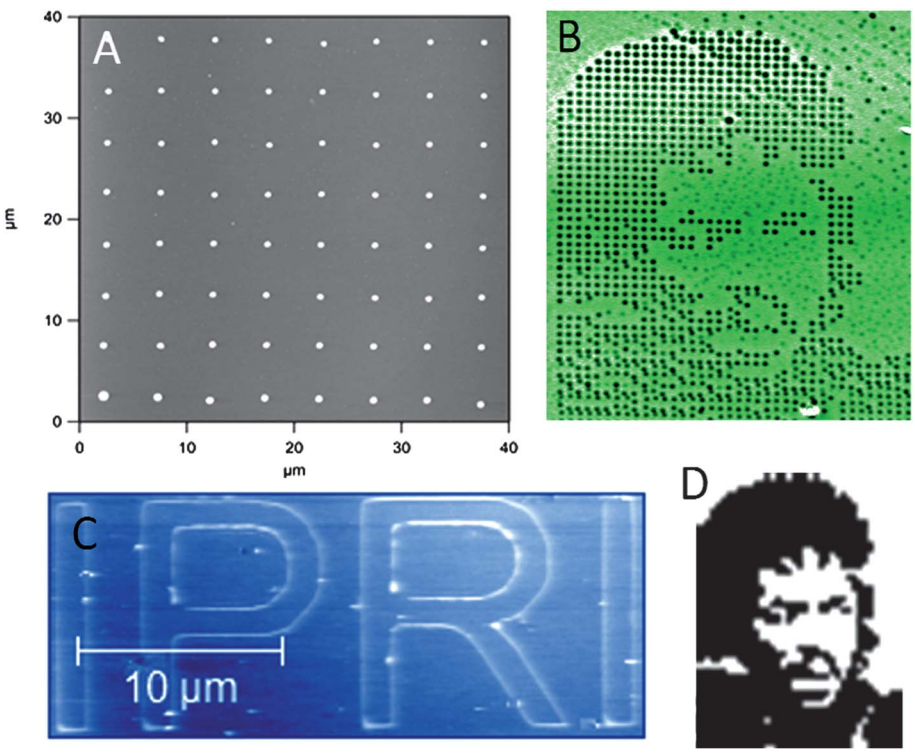

Fig. 14 Sub-micron patterning, using a homemade (A) and modified commercial PEDOT/PSS ink using DPN (B), of scanned image of Jimmy Hendricks (D). DPN "writing" of IPRI (Intelligent Polymer Research Institute) (C) using a chemical oxidant ink. Line widths ≈ 100–200 nm. Previously published images are reproduced with permission.

the patterning process. This has been demonstrated for polythiophene materials on insulating and semiconducting substrates.[258] Our laboratories have recently explored the patterning of PEDOT:PSS inks onto a variety of substrates,[259] including flexible substrates (*e.g.* polyethylene terephthalate and silicone gum), and the feasibility of patterning chemical oxidants for subsequent vapour phase polymerization.[271] Fine control overpatterning of the PEDOT:PSS and chemical oxidant is promising with dot diameters and line widths down to 150 nm achieved (Fig. 14).

In essence, DPN represents a new brand of non-traditional fabrication approaches identified as being critical for producing complex nanomaterials and nanostructures. It is capable of filling the "nanometre resolution" void in current liquid ink dispensing technologies (*e.g.* inkjet printing) whose patterning is limited to microscale resolution. Recently, high-throughput patterning and scale-up methods using polymer-pen[260] or beam-pen[261] have been developed and, hence, DPN is continuing to evolve as an advanced and practical nanolithography technique.

The different capabilities of fibre spinning and printing technologies and other nanolithography techniques such as DPN are collectively forming an integral and unique set of micro- and nano-fabrication tools for manipulating OCP nanomaterials, particularly those in the form of solution material dispersions and liquid inks. Each of these fabrication techniques alone will not necessarily satisfy the requirements for a device, but together they pose a powerful route to assembling complex 3D structures. This is important for medical bionics devices requiring a high level of integration and control over the material properties at the bulk, micro- and nano-domains.

5.2 Nano-biocharacterisation

The electromaterial–cellular interface is a complex and multifaceted environment through which a suite of interactions act in concert to guide biomolecular and cellular function. Research has judiciously turned towards developing an understanding of the fundamental mechanisms at the electromaterial–cellular interface, particularly the ability to interface effectively, and specifically control protein-mediated and cellular interactions. However, deducing a level of molecular detail from macroscopic and whole cell observations is difficult and we are only just beginning to gain insight into the effect of dynamic, nanoscale properties of electromaterials as a function of electrical stimulation. This is where characterization techniques, such as those based on Biological-Atomic Force Microscopy (Bio-AFM), that have the ability to collect topographical, chemical, mechanical and electrical information with unprecedented resolution in biologically relevant environments, present exciting opportunities for looking into the nanodomain.

The ability of AFM to probe molecular lengthscales relevant to protein interactions relies on its operation of directly interacting with a surface *via* a nanometer-sized tip (typically 5–20 nm in radius) mounted on a flexible cantilever capable of recording piconewton forces. In addition to raster scanning the probe across the surface to build up a 3D topographic image, approaching and retracting the tip at a single x–y position while monitoring the displacement of the cantilever enables forces such as adhesion to be measured as a function of the distance from the surface (*i.e.* force–distance curve).[262] These measurements can be conducted in fluids, thus opening up the exploration of biomolecular and protein interactions in near physiological and biologically relevant environments.

With lateral imaging resolution capabilities of 1–2 nm, AFM imaging studies have directly visualized the nanoscale interaction of single living cell machinery (*e.g.* neurite, focal adhesions) with respect to the underlying nanostructured topography. Specifically for OCP based materials, the mechanism underlying the contact guidance of neurite outgrowth by electrospun fibres has been explored using the high resolution capabilities of AFM[179] (Fig. 15). Finger-like lateral projections, or filopodia, were observed to project outward in a perpendicular direction from a single neurite adjacent to a PPy/SIBS fibre (Fig. 15C). These projections made intimate contact with the fibre and only extended from the side of the neurite directly opposing the fibre. There also appeared to be regions where the filopodia continuously projected at intervals perpendicular to extending neurites, assisting the neurite to sense and maintain its proximity to the fibre. The neurites elongated adjacent to the fibre, or on top of the fibre, rather than traversing the fibre. These observations revealed that the contact guidance occurred at the level of

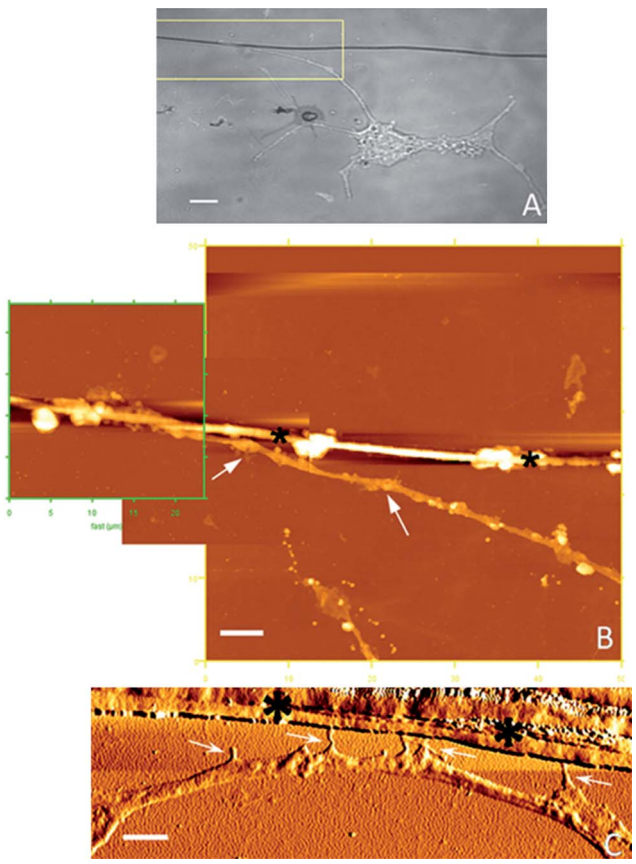

Fig. 15 (A) Optical and (B) corresponding AFM images of the boxed region in (A) showing a neurite (arrows) extending along a PPy/SIBS fibre (black asterisks). Scale bar in (A) = 20 μm. Scale bar in (B) = 5 μm. (C) High resolution AFM image showing small finger-like lateral outgrowths (arrows) making contact with a PPy/SIBS fibre (black asterisks). Scale bar in (C) = 1 μm. (Reproduced with permission from ref. 179.)

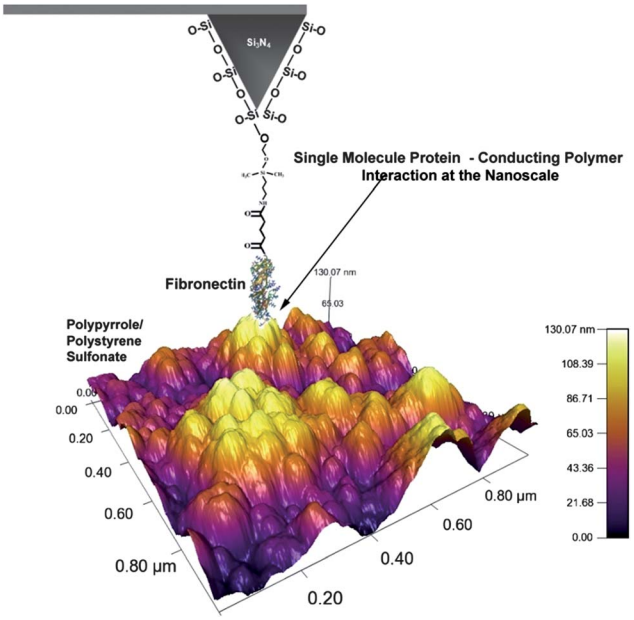

Fig. 16 Schematic of protein functionalized AFM tip interacting with a polypyrrole film doped with polystyrene sulfonate. The depicted tip functionalization is fibronectin covalently linked to an amino-coated tip *via* glutaraldehyde cross-linking. The 3-D topographic polypyrrole film is obtained from AFM imaging. The interaction between the single protein and nanometer topographic features of the polymer (the interaction is depicted roughly to scale) is measured as the AFM tip maps the forces across the surface.

micron-scale neurite elongation and alignment and at the nanoscale level of filopodia "sensing".

Through a variety of strategies to chemically functionalize the AFM tip, the subsequent attachment of many different proteins in active and desired conformations has made it possible to directly measure the forces between a single protein and substrate of interest. This has spawned a new and exciting area termed 'force spectroscopy' utilizing analysis of the force–distance curves to provide information on single protein bond(s) kinetics, binding probabilities and mechanisms for ligand–receptor (protein) interactions,[263] protein interactions with model substrates having well-defined surface functional groups (*e.g.* self-assembled monolayers)[264] and surfaces of more complex polymer surfaces.[265]

AFM force spectroscopy has shown it is possible to deconvolute the effects of the intrinsic surface heterogeneity of OCPs, as any given single x–y location of a force–distance curve can actually represent a specific single protein–surface interaction bearing its own characteristic fingerprint. This approach provides a means to understand the interactions between the OCP and extracellular matrix proteins such as fibronectin (Fn), which are currently implicated in the underlying abilities of OCP to control cell attachment and growth. The principle behind this type of force spectroscopy experiment is depicted in Fig. 16 and highlights the ability to probe protein–OCP interactions both at the (biological) molecular and (material) nanometer scale. Preliminary results on PPy–Fn interactions indicate that the measured forces can be related back to interacting groups on the protein and surface groups (*e.g.* dopants), even with details at the sub-molecular level.[266] Even if the specific binding of proteins is not resolved, the degree of binding strength can be quantified as has been previously demonstrated for the interaction of a T59 phage peptide sequence (attached to the tip) and polypyrrole/chloride film.[267]

Having demonstrated the specific binding of proteins to dopants and/or their binding strengths, the use of Bio-AFM in this area in combination with integrated fluorescent techniques is expected to contribute to the rational design of OCPs for biomaterial applications. It also has the credentials to deduce the molecular details of protein– and cellular–electromaterial interactions, which is currently tantalising researchers in the field.

6. Conclusions

The impact of nanostructuring mechanical and electrical properties of electrodes is critically dependant on the electrode composition. The observed effects are also dependant on the geometry of the nanosized features. Nanostructuring enhances surface area providing increased sites of adhesion and also plays a critical role in cell proliferation and tissue acceptance.

It is recognized that many cell types react to nanofeatures in a variety of ways including cell adhesion, proliferation, morphology and gene expression. Inevitably, the emergence of nanostructured electromaterials enables several degrees of control over the cascade of molecular and cellular events initiated by implanting electrodes into the body for bionic applications. As we take time to refine strategies that enable the assembly of structures with control over the spatial distribution of composition, function and physical (electronic and mechanical) properties in three dimensions with nanometre resolution, then our ability to engineer the biomolecular and cellular events that control the nature of the electrode–cellular interface will be dramatically enhanced. This requires an intergrated approach to the development of processable formulations and innovative "machinery" for fabrication. We must also confront the fact that current materials characterisation tools are not adequate. We require the ability to characterise 3D structures with nanometre resolution.

Nanotechnology, by design, is yet to have a significant impact on clinical applications of medical bionics. However, it is likely that previous manufacturing or pretreatment protocols has inadvertently introduced nanostructure leading to improved performance. As we increase our fabrication capabilities to build practical devices from the nanodomain applications in the clinical world will undoubtedly accelerate and new applications for medical bionics emerge.

Acknowledgements

The authors wish to acknowledge the ongoing financial support of the Australian Research Council and National Health and Medical Research Council. The authors also gratefully acknowledge Mr Cameron Ferris for his comments during the preparation of the manuscript.

References

1 G. M. Clark, *Philos. Trans. R. Soc., B*, 2006, **361**, 791–810.
2 R. Elmquist and P. Senning, *Proceedings of the 2nd International Conference on Medical Electronics*, ed. C. N. Smyth, Iliffe & Sons, London, 1960.

3 A. Kirchner, F. Birklein, H. Stefan and H. O. Handwerker, *Neurology*, 2005, **55**, 1167–1171.
4 P. C. Collins, *Proc. Inst. Med. Chicago*, 1985, **35**, 74–76.
5 X. Sui, L. Li, X. Chai, K. Wu, C. Zhou, X. Sun, X. Xu, X. Li and R. Qiushi, in *Implantable Neural Prostheses 1*, ed. D. D. Zhou and E. Greenbaum, Springer, Germany, 2006, pp. 43–85.
6 A. L. Benabid, *Curr. Opin. Neurobiol.*, 2003, **13**, 696–706.
7 G. G. Wallace, S. E. Moulton and G. M. Clark, *Science*, 2009, **324**, 185–186.
8 P. Elter, R. Lange and U. Beck, *Colloids Surf., B*, 2011, **89**, 139–146.
9 K. A. Power, K. T. Fitzgerald and W. M. Gallagher, *Biomaterials*, 2010, **31**, 6667–6674.
10 L. A. Cyster, K. G. Parker, T. L. Parkerand and D. M. Grant, *Biomaterials*, 2004, **25**, 97–107.
11 E. K. F. Yim, R. M. Reano, S. W. Pang, A. F. Yee, C. S. Chen and K. W. Leong, *Biomaterials*, 2005, **26**, 5405–5413.
12 L. Yang, V. Chinthapenta, Q. Li, D. Stout, A. Liang, B. W. Sheldon and T. J. Webster, *J. Biomed. Mater. Res., Part A*, 2011, **97**, 375–382.
13 A. Thapa, D. C. Miller, T. J. Webster and K. M. Haberstroh, *Biomaterials*, 2003, **24**, 2915–2926.
14 A. S. Andersson, F. Backhed, A. von Euler, A. Richter-Dahlfors, D. Sutherland and B. Kasemo, *Biomaterials*, 2003, **24**, 3427–3436.
15 M. J. Dalby, M. O. Riehle, D. S. Sutherland, H. Agheli and A. S. Curtis, *Biomaterials*, 2004, **25**, 5415–5422.
16 M. M. Shokrieh and R. Rafiee, *Mech. Compos. Mater.*, 2010, **46**, 155–172.
17 J. N. Barisci, R. Stella, G. M. Spinks and G. G. Wallace, *Electrochim. Acta*, 2000, **46**, 519–531.
18 K. D. O'Neil, B. Shaw and O. A. Semenikhin, *J. Phys. Chem. B*, 2007, **111**, 9253–9269.
19 H. He, J. Zhu, N. J. Tao, L. A. Nagahara, I. Amlani and R. Tsui, *J. Am. Chem. Soc.*, 2001, **123**, 7730–7731.
20 F. A. Spelman, *Audiol. Neurotol.*, 2006, **11**, 77.
21 J. L. R. Martin and E. Martin-Sanchez, *Eur. Psychiatr.*, 2012, **27**, 147–155.
22 B. Majkowska-Zwolinska, P. Zwolinski, M. Roszkowski and K. Drabik, *Childs Nerv. Syst.*, 2012, **28**, 621–628.
23 P. Cristancho, M. A. Cristancho, G. H. Baltuch, M. E.Thase and J. P. O'Reardon, *J. Clin. Psychiatry*, 2011, **72**, 1376–1382.
24 T. Biermann, S. Kreil, T. W. Groemer, C. Maihofner, T. Richter-Schmiedinger, J. Kornhuber and W. Sperling, *Pharmacopsychiatry*, 2011, **44**, 179–182.
25 E. Ben-Menachem and J. French, *Epileptic Disord.*, 2005, **7**(suppl. 1), 22–26.
26 D. Labar, *Seizure*, 2004, **13**, 392–398.
27 M. Nei, M. O'Connor, J. Liporace and M. Sperling, *Epilepsia*, 2006, **47**, 115–122.
28 A. Handforth, C. M. DeGiorgio, S. C. Schachter, B. M. Uthman, D. K. Naritoku, E. S. Tecoma, T. R. Henry, S. D. Collins, B. V. Vaughn, R. C. Gilmartin, D. R. Labar, G. L. Morris, III, M. C. Salinsky, I. Osorio, R. K. Ristanovic, D. M. Labiner, J. C. Jones, J. V. Murphy, G. C. Ney and J. W. Wheless, *Neurology*, 1998, **51**, 48–55.
29 C. M. DeGiorgio, S. C. Schachter, A. Handforth, M. Salinsky, J. Thompson, B. Uthman, R. Reed, S. Collin, E. Tecoma, G. L. Morris, B. Vaughn, D. K. Naritoku, T. Henry, D. Labar, R. Gilmartin, D. Labiner, I. Osorio, R. Ristanovic, J. Jones, J. Murphy, G. Ney, J. Wheless, P. Lewis and C. Heck, *Epilepsia*, 2000, **41**, 1195–1200.
30 P. Mohr, M. Rodriguez, A. Slavickova and J. Hanka, *Neuropsychobiology*, 2011, **64**, 170–181.
31 J. F. Rizzo and J. Wyatt, *Neuroscientist*, 1997, **3**, 251–262.
32 W. Liu, E. McGucken, K. Vichienchom, S. M. Clements, S. C. Demarco, M. Humayun, E. Juan, J. Weiland and R. Greenberg, *Proc. IEEE Int. Conf. Syst., Man., Cyber.*, 1999, **4**, 364–369.
33 M. S. Humayun, J. D. Weiland, G. Y. Fujii, R. Greenberg, R. Williamson, J. Little, B. Mech, V. Cimmarusti, G. Van Boemel, G. Dagnelie and E. J. de Juan, *Vis. Res.*, 2003, **43**, 2573–2581.
34 C. Veraart, C. Raftopoulos, J. T. Mortimer, J. Delbeke, D. Pins, G. Michaux, A. Vanlierde, S. Parrini and M. C. Wanet-Defalque, *Brain Res.*, 1998, **813**, 181–186.
35 J. Delbeke, M. Oozeer and V. Claude, *Vis. Res.*, 2003, **43**, 1091–1102.
36 X. Sui, L. Li, X. Chai, K. Wu, C. Zhou, X. Sun, X. Xu, X. Li and R. Qiushi, Visual Prosthesis for Optic Nerve Stimulation, in *Implantable Neural Prostheses 1*, ed. D. D. Zhou and E. Greenbaum, Springer, Germany, 2009, pp. 43–85.
37 W. H. Dobelle, M. G. Mladejovsky and J. P. Girvin, *Science*, 1974, **183**, 440–444.
38 R. A. Normann, E. M. Maynard, P. J. Rousche and D. J. Warren, *Vis. Res.*, 1999, **39**, 2577–2587.
39 G. S. Brindley and W. S. Lewin, *J. Physiol.*, 1968, **196**, 479–493.
40 D. R. Merrill, M. Bikson and J. G. R. Jefferys, *J. Neurosci. Methods*, 2005, **141**, 171–198.
41 M. A. Nitsche, D. Liebetanz, N. Lang, A. Antal, F. Tegau and W. Paulus, *Clin. Neurphysiol.*, 2004, **114**, 2220–2222.
42 S. F. Cogan, *Annu. Rev. Biomed. Eng.*, 2008, **10**, 275–309.
43 E. J. Tehovnik, *J. Neurosci. Methods*, 1996, **65**, 1–17.
44 X. T. Cui and D. D. Zhou, *IEEE Trans. Neural. Syst. Rehabil. Eng.*, 2007, **15**, 502–508.
45 R. A. Green, N. H. Lovell, G. G. Wallace and L. A. Poole-Warren, *Biomaterials*, 2008, **29**, 3393–3399.
46 E. W. Keefer, B. R. Botterman, M. I. Romero, A. F. Rossi and G. W. Gross, *Nat. Nanotechnol.*, 2008, **3**, 434–439.
47 K. Wang, H. A. Fishman, H. Dai and J. S. Harris, *Nano Lett.*, 2006, **9**, 2043–2048.
48 N. A. Kotov, J. O. Winter, I. P. Clements, E. Jan, B. P. Timko, S. Campidelli, S. Pathak, A. Mazzatenta, C. M. Lieber, M. Prato, R. V. Bellamkonda, G. A. Silva, N. W. S. Kam, F. Patolsky and L. Ballerini, *Adv. Mater.*, 2009, **21**, 1–35.
49 I. Gotman, *J. Endourol.*, 1997, **11**, 383–389.
50 D. A. Robinson, *Proc. IEEE*, 1968, **56**, 1065–1071.
51 G. S. Attard, P. N. Barlett, N. R. B. Coleman, J. M. Elloit, J. R. Owen and J. Wang, *Science*, 1997, **278**, 838–840.
52 K. S. Choi, E. W. McFarland and G. D. Stucky, *Adv. Mater.*, 2003, **15**, 2018–2021.
53 S. Park, Y. J. Song, J. H. Han, H. Boo and T. D. Chung, *Electrochim. Acta*, 2010, **55**, 2029–2035.
54 S. Park, Y. J. Song, H. Boo and T. D. Chung, *J. Phys. Chem. C*, 2010, **114**, 8721–8726.
55 S. S. Thanawala, R. J. Baird, D. G. Georgiev and G. W. Auner, *Appl. Surf. Sci.*, 2008, **254**, 5164–5169.
56 M. Carballo-Vila, B. Moreno-Burriel, E. Chinarro, J. R. Jurado, N. Casañ-Pastor and J. E. Collazos-Castro, *J. Biomed. Mater. Res., Part A*, 2009, **90**, 94–105.
57 M. Heim, B. Yvert and A. Kuhn, *J. Physiol.*, 2011, DOI: 10.1016/j.jphysparis.2011.10.001.
58 Y. Lu, T. Wang, Z. Cai, Y. Cao, H. Yang and Y. Y. Duan, *Sens. Actuators, B*, 2008, **137**, 334–339.
59 Y. Lu, Z. Cai, Y. Cao, H. Yang and Y. Y. Duan, *Electrochem. Commun.*, 2008, **10**, 778–782.
60 S. B. Jun, M. R. Hynd, K. L. Smith, J. K. Song, J. N. Turner, W. Shain and S. J. Kim, *Med. Biol. Eng. Comput.*, 2007, **45**, 1015–1021.
61 J. M. Elloit and J. R. Owen, *Phys. Chem. Chem. Phys.*, 2000, **2**, 5653–5659.
62 S. A. Desai, J. D. Rolston, L. Guo and S. M. Potter, *Front. Neuroeng.*, 2010, **3**, 1–11.
63 C. T. J. Low, M. de la Toba and F. C. Walsh, *Trans. Inst. Met. Finish.*, 2011, **89**, 44–50.
64 K. S. Brammer, S. Oh, J. O. Gallagher and S. Jin, *Nano Lett.*, 2008, **8**, 786–793.
65 T. Sjöström, M. J. Dalby, A. Hart, R. Tare, R. O. C. Oreffo and B. Su, *Acta Biomater.*, 2009, **5**, 1433–1441.
66 H. Yoon, P. Hankins, S. Oh, R. E. Harbaugh and V. K. Varadan, *J. Nanotechnol. Eng. Med.*, 2010, **1**, 021006.
67 S. Hackwood, L. M. Schiavone, W. C. Dautremont-Smith and G. Beni, *J. Electrochem. Soc.*, 1981, **128**, 2569–2573.
68 S. F. Cogan, J. Ehrlich, T. D. Plante, A. Smirnov, D. B. Shire, M. Gingerich and J. F. Rizzo, *J. Biomed. Mater. Res., Part B*, 2009, **89**, 353–361.
69 S. Negia, R. Bhandari, L. Rieth, R. V. Wagenen and F. Solzbacher, *J. Neurosci. Methods*, 2010, **186**, 8–17.
70 W. L. C. Rutten, *Annu. Rev. Biomed. Eng.*, 2002, **4**, 407–452.
71 A. Norlin, J. Pan and C. Leygraf, *J. Electrochem. Soc.*, 2005, **152**, J7–J15.
72 C. de Haro, R. Mas, G. Abadal, J. Muñoz, F. Perez-Murano and C. Domíguez, *Biomaterials*, 2002, **23**, 4515–4521.

73 L. M. Dai, A. Patil, X. Gong, Z. Guo, L. Liu, Y. Liu and D. Zhu, *ChemPhysChem*, 2003, **4**, 1150–1169.
74 A. M. Cassell, N. R. Franklin, T. W. Tombler, E. M. Chan, J. Han and H. Dai, *J. Am. Chem. Soc.*, 1999, **121**, 7975–7976.
75 W. Z. Li, S. S. Xie, L. X. Qian, B. H. Chang, B. S. Zou, W. Y. Zhou, R. A. Zhao and G. Wang, *Science*, 1996, **274**, 1701–1703.
76 S. H. Tsai, C. T. Shiu, S. H. Lai, L. H. Chan, W. Hsieh and H. C. Shih, *J. Mater. Sci. Lett.*, 2002, **21**, 1709–1711.
77 X. Nan, Z. Gu and Z. Liu, *J. Colloid Interface Sci.*, 2002, **245**, 311–318.
78 Y. Yang, S. Huang, H. He, A. W. H. Mau and L. Dai, *J. Am. Chem. Soc.*, 1999, **121**, 10832–10833.
79 J. Chen, Y. Liu, A. I. Minett, C. Lynam, J. Wang and G. G. Wallace, *Chem. Mater.*, 2007, **19**, 3595.
80 J. Chen, J. Z. Wang, A. I. Minett, Y. Liu, C. Lynam, H. Liu and G. G. Wallace, *Energy Environ. Sci.*, 2009, **2**, 393.
81 J. Chen, Y. Liu, A. I. Minett, C. Lynam, J. Wang and G. G. Wallace, *Chem. Mater.*, 2007, **19**, 3595–3597.
82 D. Antiohos, S. E. Moulton, A. I. Minett, G. G. Wallace and J. Chen, *Electrochem. Commun.*, 2010, **12**, 1471–1474.
83 Y. Y. Tan, K. D. G. I. Jayawardena, A. A. D. T. Adikaari, L. W. Tan, J. V. Anguita, S. J. Henley, V. Stolojan, J. D. Carey and S. R. P. Silva, *Carbon*, 2012, **50**, 668–673.
84 A. Reina, X. Jia, J. Ho, D. Nezich, H. Son, V. Bulovic, M. S. Dresselhaus and J. Kong, *Nano Lett.*, 2009, **9**, 30–35.
85 X. Li, W. Cai, J. An, S. Kim, J. Nah, D. Yang, R. Piner, A. Velamakanni, I. Jung, E. Tutuc, S. K. Banerjee, L. Colombo and R. S. Ruoff, *Science*, 2009, **324**, 1312–1324.
86 W. Li, C. Tan, M. A. Lowe, H. D. Abruna and D. C. Ralph, *ACS Nano*, 2011, **5**, 2264–2270.
87 C. Lynam, A. L. Minett, S. E. Habas, S. Gambhir, D. L. Officer and G. G. Wallace, *Int. J. Nanotechnol.*, 2008, **5**, 331–351.
88 M. F. Islam, E. Rojas, D. M. Bergey, A. T. Johnson and A. G. Yodh, *Nano Lett.*, 2003, **3**, 269–273.
89 B. Vigolo, A. Penicaud, C. Coulon, C. Sauder, R. Pailler, C. Jounet, P. Bernier and P. Poulin, *Science*, 2000, **290**, 1331–1334.
90 O. Regev, P. N. B. ElKati, J. Loos and C. E. Koning, *Adv. Mater.*, 2004, **16**, 248–251.
91 M. A. Hamon, M. E. Itkis, S. Niyogi, T. Alvaraez, C. Kuper, M. Menon and R. C. Haddon, *J. Am. Chem. Soc.*, 2001, **123**, 11292.
92 J. Zhang, J. K. Lee, Y. Wu and R. W. Murray, *Nano Lett.*, 2003, **3**, 403–407.
93 J. N. Coleman, A. B. Dalton, S. Curran, A. Rubio, A. P. Davey, A. Drury, B. McCarthy, B. Lahr, P. M. Ajayan, S. Roth, R. C. Barklie and W. J. Blau, *Adv. Mater.*, 2000, **12**, 213.
94 M. Giulianini, E. R. Waclawik, J. M. Bell, M. De Crescenzi, P. Castrucci, M. Scarselli and N. Motta, *Appl. Phys. Lett.*, 2009, **95**, 013304.
95 Y. K. Kang, O.-S. Lee, P. Deria, S. H. Kim, T.-H. Park, D. A. Bonnell, J. G. Saven and M. J. Therien, *Nano Lett.*, 2009, **9**, 1414–1418.
96 Y. Kang and T. A. Taton, *J. Am. Chem. Soc.*, 2003, **125**, 5650–5651.
97 S. W. Kim, T. Kim, Y. S. Kim, H. S. Choi, H. J. Lim, S. J. Yang and C. R. Park, *Carbon*, 2012, **50**, 3–33.
98 S. E. Moulton, M. Maugey, P. Poulin and G. G. Wallace, *J. Am. Chem. Soc.*, 2007, **129**, 9452–9457.
99 C. Lynam, S. E. Moulton and G. G. Wallace, *Adv. Mater.*, 2007, **19**, 1244–1248.
100 S. E. Moulton, A. I. Minett, R. Murphy, K. P. Ryan, D. McCarthy, J. N. Coleman, W. J. Blau and G. G. Wallace, *Carbon*, 2005, **43**, 1879–1884.
101 C. J. Ferris and M. in het Panhuis, *Soft Matter*, 2009, **5**, 1466–1473.
102 Q. Y. Guo, J. Y. Shao, T. Sun, H. Li, S. Lan and Z. H. Xu, *Electrochim. Acta*, 2011, **56**, 1432–1438.
103 D. O. Demirkol and S. Timur, *Microchim. Acta*, 2011, **173**, 537–542.
104 S. Taeger and M. Mertig, *Int. J. Mater. Res.*, 2007, **98**, 742–748.
105 S. Stankovich, D. A. Dikin, R. D. Piner, K. A. Kohlhaas, A. Kleinhammes, Y. Jia, Y. Wu, S. T. Nguyen and R. S. Ruoff, *Carbon*, 2007, **45**, 1558–1565.
106 D. Li, M. B. Mueller, S. Gilje, R. B. Kaner and G. G. Wallace, *Nat. Nanotechnol.*, 2008, **3**, 101–105.
107 P. Blake, P. D. Brimicombe, R. R. Nair, T. J. Booth, D. Jiang, F. Schedin, L. A. Ponomarenko, S. V. Morozov, H. F. Gleeson, E. W. Hill, A. K. Geim and K. S. Novoselov, *Nano Lett.*, 2008, **8**, 1704–1709.
108 Y. Hernandez, V. Nicolosi, M. Lotya, F. M. Blighe, Z. Sun, S. De, I. T. McGovern, B. Holland, M. Byrne, Y. K. Gun'Ko, J. J. Boland, P. Niraj, G. Duesberg, S. Krishnamurthy, R. Goodhue, J. Hutchison, V. Scardaci, A. C. Ferrari and J. N. Coleman, *Nat. Nanotechnol.*, 2008, **3**, 563–568.
109 M. Lotya, Y. Hernandez, P. J. King, R. J. Smith, V. Nicolosi, L. S. Karlsson, F. M. Blighe, S. De, Z. Wang, I. T. McGovern, G. S. Duesberg and J. N. Coleman, *J. Am. Chem. Soc.*, 2009, **131**, 3611–3620.
110 S. Park, J. An, I. Jung, R. D. Piner, S. J. An, X. Li, A. Velamakanni and R. S. Ruoff, *Nano Lett.*, 2009, **9**, 1593–1597.
111 V. C. Tung, M. J. Allen, Y. Yang and R. B. Kaner, *Nat. Nanotechnol.*, 2009, **4**, 25–29.
112 S. Stankovich, R. D. Piner, X. Q. Chen, N. Q. Wu, S. T. Nguyen and R. S. Ruoff, *J. Mater. Chem.*, 2006, **16**, 155.
113 Y. Xu, H. Bai, G. Lu, C. Li and G. Shi, *J. Am. Chem. Soc.*, 2008, **130**, 5856–5857.
114 R. Hao, W. Qian, L. Zhang and Y. Hou, *Chem. Commun.*, 2008, 6576.
115 M. Lotya, Y. Hernandez, P. J. King, R. J. Smith, V. Nicolosi and L. S. Karlsson, *et al.*, *J. Am. Chem. Soc.*, 2009, **131**, 3611–3620.
116 A. B. Bourlinos, V. Georgakilas, R. Zboril, T. A. Steriotis and A. K. Stubos, *Small*, 2009, **5**, 1841–1845.
117 S. Vadukumpully, J. Paul and S. Valiyaveettil, *Carbon*, 2009, **47**, 3288–3294.
118 A. B. Bourlinos, V. Georgakilas, R. Zboril, T. A. Steriotis, A. K. Stubos and C. Trapalis, *Solid State Commun.*, 2009, **149**, 2172–2176.
119 J. Liu, A. G. Rinzler, H. Dai, J. H. Hafner, R. K. Bradley, P. J. Boul, A. Lu, T. Iverson, K. Shelimov, C. B. Huffman, F. Rodriguez-Macias, Y. S. Shon, T. Randall Lee, D. T. Colbert and R. E. Smalley, *Science*, 1998, **280**, 1253–1256.
120 J. N. Coleman, W. J. Blau, A. B. Dalton, E. Munoz, S. Collins, B. G. Kim, J. Razal, M. Selvidge, G. Vieiro and R. H. Baughman, *Appl. Phys. Lett.*, 2003, **82**, 1682–1684.
121 J. N. Barisci, G. G. Wallace, D. Chattopadhyay, F. Papadimitrakopoulos and R. H. Baughman, *J. Electrochem. Soc.*, 2003, **150**, 409–413.
122 H. Chen, M. B. Muller, K. J. Gilmore, G. G. Wallace and D. Li, *Adv. Mater.*, 2008, **20**, 3557–3562.
123 X. W. Yang, L. Qiu, C. Cheng, Y. Z. Wu, Z. F. Ma and D. Li, *Angew. Chem., Int. Ed.*, 2011, **50**, 7325–7328.
124 L. Qiu, X. Yang, X. Gou, W. Yang, Z.-F. Ma, G. G. Wallace and D. Li, *Chem.–Eur. J.*, 2010, **16**, 10653–10658.
125 C. Y. Su, A. Y. Law, Y. L. Chen, C. Y. Wei, C. H. Weng, P. C. Wang, F. R. Chen, K. C. Leon and C. H. Tsai, *J. Phys. Chem. C*, 2010, **114**, 11588–11594.
126 Y. Mao, Y. Bao, W. Wang, Z. Li, F. Li and L. Niu, *Talanta*, 2011, **85**, 2106–2112.
127 X. Wang, J. F. Wang, H. J. Cheng, P. Yu, J. S. Ye and L. Q. Mao, *Langmuir*, 2011, **27**, 11180–11186.
128 C. Y. Deng, J. H. Chen, Z. Nie and S. H. Si, *Biosens. Bioelectron.*, 2010, **26**, 213–219.
129 Q. A. Gao, Y. Y. Guo, W. Y. Zhang, H. L. Qi and C. X. Zhang, *Sens. Actuators, B*, 2011, **153**, 219–225.
130 M. N. Zhang, K. P. Gong, H. W. Zhang and L. Q. Mao, *Biosens. Bioelectron.*, 2005, **20**, 1270–1276.
131 H. F. Cui, Y. H. Cui, Y. L. Sun, K. Zhang and W. D. Zhang, *Nanotechnology*, 2010, **21**, 15601.
132 F. Li, M. Xue, X. Ma, M. Zhang and T. Cao, *Anal. Chem.*, 2011, **83**, 6426–6430.
133 Z. Zhen, Y. M. Lin, M. J. Rooks and P. Avouris, *Physica E*, 2007, **40**, 228–232.
134 M. Y. Han, B. Ozyilmaz, Y. Zhang and P. Kim, *Phys. Rev. Lett.*, 2007, **98**, 206805–206809.
135 L. Tapaszto, G. Dobrik, P. Lambin and L. P. Biro, *Nat. Nanotechnol.*, 2008, **3**, 397–402.
136 B. Li, G. Lu, X. Z. Zhou, X. H. Cao, F. Boey and H. Zhang, *Langmuir*, 2009, **25**, 10455–10458.
137 Y.-S. Shin, J. Y. Son, M.-H. Jo, Y.-H. Shin and H. M. Jang, *J. Am. Chem. Soc.*, 2011, **133**, 5623–5625.
138 H. Li, X. H. Cao, B. Li, X. Z. Zhou, G. Lu, C. Liusman, Q. Y. He, F. Boey, S. S. Venkatraman and H. Zhang, *Chem. Commun.*, 2011, **47**, 10070–10072.

139 R. Sen, B. Zhao, D. Perea, M. E. Itkis, H. Hu, J. Love, E. Bekyarova and R. C. Haddon, *Nano Lett.*, 2004, **4**(3), 459–464.
140 H. Hou, J. J. Ge, J. Zeng, Q. Li, D. H. Reneker, A. Greiner and S. Z. D. Cheng, *Chem. Mater.*, 2005, **17**, 967–973.
141 J. Jason, J. J. Ge, H. Hou, Q. Li, M. J. Graham, A. Greiner, D. H. Reneker, F. W. Harris and C. Z. D. Cheng, *J. Am. Chem. Soc.*, 2004, **126**, 15754–15761.
142 C. Kim, K. S. Yang, M. Kojima, K. Yoshida, Y. J. Kim, Y. A. Kim and M. Endo, *Adv. Funct. Mater.*, 2006, **16**, 2393–2397.
143 C. Seoul, Y. T. Kim and C. K. Baek, *J. Polym. Sci., Part B: Polym. Phys.*, 2003, **41**, 1572–1577.
144 N. Zhu, W. Liu, M. Q. Xue, Z. A. Xie, D. Zhou, M. N. Zhang, J. T. Chen and T. B. Cao, *Electrochim. Acta*, 2010, **55**, 5813–5818.
145 H. Niu, T. Lin and X. Wang, *J. Appl. Polym. Sci.*, 2009, **114**, 3524–3530.
146 J. M. Razal, K. J. Gilmore and G. G. Wallace, *Adv. Funct. Mater.*, 2008, **18**, 61–66.
147 G. M. Spinks, S. R. Shin, G. G. Wallace, P. G. Whitten, I. Y. Kim, S. I. Kim and S. J. Kim, *Sens. Actuators, B*, 2007, **121**, 616–621.
148 A. J. Granero, J. M. Razal, G. G. Wallace and M. in het Panhuis, *J. Mater. Chem.*, 2010, **20**, 7953–7956.
149 A. J. Granero, J. M. Razal, G. G. Wallace and M. in het Panhuis, *Adv. Funct. Mater.*, 2008, **18**, 3759–3764.
150 K. J. Gilmore, M. Kita, Y. Han, A. Gelmi, M. J. Higgins, S. E. Moulton, G. M. Clark, R. M. I. Kapsa and G. G. Wallace, *Biomaterials*, 2009, **30**, 5292–5304.
151 J. H. Collier, J. P. Camp, T. W. Hudson and C. E. Schmidt, *J. Biomed. Mater. Res.*, 2000, **50**, 574–584.
152 X. Yang, C. O. Too, L. Sparrow, J. Ramshaw and G. G. Wallace, *React. Funct. Polym.*, 2000, **53**, 53–62.
153 B. C. Thompson, S. E. Moulton, R. T. Richardson and G. G. Wallace, *Biomaterials*, 2011, **32**, 3822–3830.
154 B. C. Thompson, S. E. Moulton, J. Ding, R. T. Richardson, A. Cameron, S. O'Leary, G. G. Wallace and G. M. Clark, *J. Controlled Release*, 2006, **116**, 285–294.
155 J. F. Zhang, S. J. Bao, C. M. Li, H. J. Bian, X. Q. Cui, Q. L. Bao, C. Q. Sun, J. Guo and L. R. Lian, *J. Phys. Chem. C*, 2008, **112**, 14843.
156 C. F. Zhou, X. S. Du and S. P. Ringer, *Synth. Met.*, 2010, **160**, 1636–1639.
157 K. Wang, J. Huang and Z. X. Wei, *J. Phys. Chem. C*, 2010, **114**, 8062–8067.
158 D. Wei, H. L. Wang, P. Hiralal, P. Andrew, T. Ryhanen, Y. Hayashi and G. A. J. Amaratunga, *Nanotechnology*, 2010, **21**, 35702.
159 C. F. Zhou, Z. W. Liu, Y. S. Yan, X. S. Du, Y. W. Mai and S. Ringer, *Nanoscale Res. Lett.*, 2011, **6**, 364–364.
160 M. Aldissi and S. P. Armes, *Prog. Org. Coat.*, 1991, **19**, 21–25.
161 J. Jang, J. H. Oh and G. D. Stucky, *Angew. Chem., Int. Ed.*, 2002, **41**, 4016–4019.
162 S. G. Oh and S. S. Im, *Curr. Appl. Phys.*, 2002, **2**, 273–277.
163 H. Goto and K. Akagi, *Macromol. Rapid Commun.*, 2004, **25**, 1482–1486.
164 (*a*) H. Goto and K. Akagi, *Japanese Patent*, 362979, 2002; H. Goto and K. Akagi, *Chem. Abstr.*, 2003, **139**, 344169; (*b*) H. Goto and K. Akagi, *Book of Abstracts of the International Conference of Science and Technology of Synthetic Metals*, Research Center for Theoretical Physics, Fudan University, Shanghai, China, 2002, p. 17.
165 H. Goto, N. Nomura and K. Akagi, *J. Polym. Sci., Part A: Polym. Chem.*, 2005, **43**, 4298–4302.
166 X. M. Yang, T. Y. Dai, M. Wei and Y. Lu, *Polymer*, 2006, **47**, 4596–4602.
167 W. Shi, D. T. Ge, J. X. Wang, Z. Z. Jiang, L. Ren and Q. Q. Zhang, *Macromol. Rapid Commun.*, 2006, **27**, 926–930.
168 Z. G. Qi and R. B. Lennox, *Proceedings of the Third International Symposium on Microstructures and Microfabricated Systems*, ed. P. J. Hesketh, G. Barna and H. G. Hughes, Electrochemical Society Inc, Pennington, 1997, pp. 173–178.
169 M. F. Mabrook, C. Pearson and M. C. Petty, *Sens. Actuators, B*, 2006, **115**, 547–551.
170 M. F. Mabrook, C. Pearson, M. C. Petty, J. H. Ahn, C. Wang, M. R. Bryce, P. Christie and G. G. Roberts, *Appl. Phys. Lett.*, 2005, **86**, 013507.
171 J. B. Chang, V. Liu, V. Subramanian, K. Sivula, C. Luscombe, A. Murphy, J. Liu and J. M. J. Frechet, *J. Appl. Phys.*, 2006, **100**, 014506–014507.
172 L. Setti, A. Fraleoni-Morgera, B. Ballarin, A. Filippini, D. Frascaro and C. Piana, *Biosens. Bioelectron.*, 2005, **20**, 2019–2026.
173 P. G. Campbell and L. E. Weiss, *Expert Opin. Biol. Ther.*, 2007, **7**, 1123–1127.
174 D. H. Reneker and I. Chun, *Nanotechnology*, 1996, **7**, 216–223.
175 A. Theron, E. Zussman and A. L. Yarin, *Nanotechnology*, 2001, **12**, 384.
176 A. G. MacDiarmid, W. E. Jones, Jr, I. D. Norris, J. Gao, A. T. Johnson, Jr, N. J. Pinto, J. Hone, B. Han, F. K. Ko and H. Okuzaki, *Synth. Met.*, 2001, **119**, 27–30.
177 T. S. Kang, S. W. Lee, J. Joo and J. Y. Lee, *Synth. Met.*, 2005, **153**, 61–64.
178 S. Nair, S. Natarajan and S. H. Kim, *Macromol. Rapid Commun.*, 2005, **26**, 1599–1603.
179 X. Liu, J. Chen, K. J. Gilmore, M. J. Higgins, Y. Liu and G. G. Wallace, *J. Biomed. Mater. Res., Part A*, 2010, **94**, 1004–1011.
180 A. Babel, D. Li, Y. Xia and S. A. Jenekhe, *Macromolecules*, 2005, **38**, 4705–4711.
181 A. Bianco, C. Bertarelli, S. Frisk, J. F. Rabolt, M. C. Gallazzi and G. Zerbi, *Synth. Met.*, 2007, **157**, 276–281.
182 H. Liu, C. H. Reccius and H. G. Craighead, *Appl. Phys. Lett.*, 2005, **87**, 253106.
183 D. Li, A. Babel, S. A. Jenekhe and Y. N. Xia, *Adv. Mater.*, 2004, **16**, 2062–2066.
184 R. González and N. J. Pinto, *Synth. Met.*, 2005, **151**, 275–278.
185 A. Laforgue and L. Robitaille, *Synth. Met.*, 2008, **158**, 577–584.
186 H. D. Nguyen, J. M. Ko, H. J. Kim, S. K. Kim, S. H. Cho, J. D. Nam and J. Y. Lee, *J. Nanosci. Nanotechnol.*, 2008, **8**, 4718–4721.
187 A. Laforgue and L. Robitaille, *Macromolecules*, 2010, **43**, 4194–4200.
188 M. R. Abidian, D. H. Kim and D. C. Martin, *Adv. Mater.*, 2006, **18**, 405–409.
189 M. Panapoy, M. Saengsil and B. Ksapabutr, *Adv. Mater. Res.*, 2008, **257**, 55–57.
190 S. I. Jeong, I. D. Jun, M. J. Choi, Y. C. Nho, Y. M. Lee and H. Shin, *Macromol. Biosci.*, 2008, **8**, 627–637.
191 S. Oh, K. S. Brammer, Y. S. J. Li, D. Teng, A. J. Engler, S. Chien and S. Jin, *Proc. Natl. Acad. Sci. U. S. A.*, 2009, **106**, 2130–2135.
192 S. Oh, C. Daraio, L.-H. Chen, T. R. Pisanic, R. R. Fiñones and S. Jin, *J. Biomed. Mater. Res., Part A*, 2006, **78**, 97–103.
193 L. A. Cyster, K. G. Parker, T. L. Parker and D. M. Grant, *Biomaterials*, 2004, **25**, 97–107.
194 C. P. Pennisi, C. Sevcencu, A. Dolatshahi-Pirouz, M. Foss, J. L. Hansen, A. N. Larsen, V. Zachar, F. Besenbacher and K. Yoshida, *Nanotechnology*, 2009, **20**, 385103–385112.
195 A. Dolatshahi-Pirouz, C. P. Pennisi, S. Skeldal, M. Foss, J. Chevallier, V. Zachar, P. Andreasen, K. Yoshida and F. Besenbacher, *Nanotechnology*, 2009, **20**, 095101–095110.
196 D. F. Williams and R. Roaf, *Implants in Surgery*, W. B. Saunders Co., London, 1973.
197 E. Wintermantel, J. Mayer and T. N. Goehring, Composites for Biomedical Applications, in *Concise Encyclopedia of Composite Materials*, ed. A. Mortensen, Elsevier, London, Amsterdam, 2006, p. 1050.
198 C. M. Seah, S. P. Chai and A. R. Mohamed, *Carbon*, 2011, **49**, 4613–4635.
199 Y. F. Ma, B. Wang, Y. P. Wu, Y. Huang and Y. S. Chen, *Carbon*, 2011, **49**, 4098–4110.
200 M. Mao and A. Bogaerts, *J. Phys. D: Appl. Phys.*, 2010, **43**, 15203.
201 J. O. Gallagher, K. F. McGhee, C. D. Wilkinson and M. O. Riehle, *IEEE Trans. Nanobiosci.*, 2002, **1**, 24–28.
202 H. W. Baac, J. H. Lee, J. M. Seo, T. H. Park, H. Chung, S.-D. Lee and S. J. Kim, *Mater. Sci. Eng., C*, 2004, **24**, 209–212.
203 T. J. Webster, C. Ergun, R. H. Doremus, R. W. Siegel and R. Bizios, *J. Biomed. Mater. Res.*, 2000, **51**, 475–483.
204 Y. Wan, Y. Wang, Z. Liu, X. Qu, B. Han, J. Bei and S. Wang, *Biomaterials*, 2005, **26**, 4453–4459.
205 M. P. Mattson, R. C. Haddon and A. M. Rao, *J. Mol. Neurosci.*, 2000, **14**, 175–182.
206 H. Hu, Y. Ni, V. Montana, R. C. Haddon and V. Parpura, *Nano Lett.*, 2004, **4**, 507–511.
207 M. A. Correa-Duarte, N. Wagenr, J. Rojas-Chapana, C. Morsczeck, M. Thie and M. Giersig, *Nano Lett.*, 2004, **4**, 2233–2236.

208 T. D. B. Nguyen-Vu, H. Chen, A. M. Cassell, R. J. Andrews, M. Meyyappan and J. Li, *IEEE Trans. Biomed. Eng.*, 2007, **54**, 1121–1128.
209 V. Lovat, D. Pantarotto, L. Lagostena, B. Cacciari, M. Grandolfo, M. Righi, G. Spalluto, M. Prato and L. Ballerini, *Nano Lett.*, 2005, **6**, 1107–1110.
210 A. Mazzatenta, M. Giugliano, S. Campidelli, L. Gambazzi, L. Businaro, H. Markram, M. Prato and L. Ballerini, *J. Neurosci.*, 2007, **27**, 6931–6936.
211 K. Matsumoto, C. Sato, Y. Naka, A. Kitazawa, R. L. D. Whitby and N. Shimizu, *J. Biosci. Bioeng.*, 2007, **103**, 216–220.
212 T. J. Rivers, T. W. Hudson and C. E. Schmidt, *Adv. Funct. Mater.*, 2002, **12**, 33–37.
213 G. Shi, Z. Zhang and M. Rouabhia, *Biomaterials*, 2008, **29**, 3792–3798.
214 J. Xie, M. R. MacEwan, S. M. Willerth, X. Li, D. W. Moran, S. E. Sakiyama-Elbert and Y. Xia, *Adv. Funct. Mater.*, 2009, **19**, 2312–2318.
215 P. R. Supronowicz, P. M. Ajayan, K. R. Ullmann, B. P. Arulanandam, D. W. Metzger and R. Bizios, *J. Biomed. Mater. Res.*, 2002, **59**, 499–506.
216 X. Li and J. Kolega, *J. Vasc. Res.*, 2002, **39**, 391–404.
217 T. J. Rivers, T. W. Hudson and C. E. Schmidt, *Adv. Funct. Mater.*, 2002, **12**, 33–37.
218 S. Shao, S. Zhou, L. Li, J. Li, C. Luo, J. Wang, X. Li and J. Weng, *Biomaterials*, 2011, **32**, 2821–2833.
219 K. Wang, J. Ruan, H. Song, J. Zhang, Y. Wo, S. Guo and C. Daxiang, *Nanoscale Res. Lett.*, 2011, **6**, 4317–4323.
220 T. R. Nayak, H. Andersen, V. S. Makam, C. Khaw, S. Bae, X. Xu, P.-L. R. Ee, J.-H. Ahn, B. H. Hong, G. Pastorin and B. Özyilmaz, *ACS Nano*, 2011, **5**, 4670–4678.
221 G.-Y. Chen, D. W.-P. Pang, S.-M. Hwang, H.-Y. Tuan and Y.-C. Hu, *Biomaterials*, 2012, **33**, 418–427.
222 S. Y. Park, J. Park, S. H. Sim, M. G. Sung, K. S. Kim, B. H. Hong and S. Hong, *Adv. Mater.*, 2011, **23**, H263–H267.
223 C. E. Schmidt, V. R. Shastri, J. P. Vacanti and R. Langer, *Proc. Natl. Acad. Sci. U. S. A.*, 1997, **94**, 8948–8953.
224 A. J. Hodgson, K. Gilmore, C. Small, G. G. Wallace, I. L. Mackenzie, T. Aoki and N. Ogata, *Supramol. Sci.*, 1994, **1**, 77–83.
225 B. Garner, A. Georgevich, A. J. Hodgson, L. Liu and G. G. Wallace, *J. Biomed. Mat. Res.*, 1999, **44**, 121–129.
226 J. Y. Wong, R. Langer and D. E. Ingber, *Proc. Natl. Acad. Sci. U. S. A.*, 1994, **91**, 3201–3204.
227 D. D. Ateh, P. Vadgama and H. A. Navsaria, *Tissue Eng.*, 2006, **12**, 645–655.
228 M. Nishizawa, H. Nozaki, H. Kaji, T. Kitazume, N. Kobayashi, T. Ishibashi and T. Abe, *Biomaterials*, 2007, **28**, 1480–1485.
229 H. Castano, E. A. O'Rear, P. S. McFetridge and V. I. Sikavitsas, *Macromol. Biosci.*, 2004, **4**, 785–794.
230 L. Zhang, W. R. Stauffer, E. P. Jane, P. J. Sammak and X. T. Cui, *Macromol. Biosci.*, 2010, **10**, 1456–1464.
231 X. T. Cui, J. Wiler, M. Dzaman, R. A. Altschuler and D. C. Martin, *Biomaterials*, 2003, **24**, 777–787.
232 X. Wang, X. T. Gu, C. Yuan, S. Chen, P. Zhang, T. Zhang, J. Yao, F. Chen and G. Chen, *J. Biomed. Mater. Res.,Part A*, 2003, **68**, 411–422.
233 J. H. Collier, J. P. Camp, T. W. Hudson and C. E. Schmidt, *J. Biomed. Mater. Res.*, 2000, **50**, 574–584.
234 R. Ravichandran, S. Sundarrajan, J. R. Venugopal, S. Mukherjee and S. Ramakrishna, *J. R. Soc., Interface*, 2010, **7**, S559–S579.
235 V. Thomas, D. R. Dean and Y. K. Vohra, *Curr. Nanosci.*, 2006, **2**, 155–177.
236 K. D. O. O'Neil and O. A. Semenikhin, *J. Phys. Chem. C*, 2007, **111**, 14823–14832.
237 A. Gelmi, M. J. Higgins and G. G. Wallace, *Biomaterials*, 2010, **31**, 1974–1983.
238 S. Liu, J. Wang, D. Zhang, P. Zhang, J. Ou, B. Liu and S. Yang, *Appl. Surf. Sci.*, 2010, **256**, 3427–3431.
239 H. J. Wang, L. W. Ji, D. F. Li and J. Y. Wang, *J. Phys. Chem. B*, 2008, **112**, 2671–2677.
240 R. M. Abidian, J. M. Corey, D. R. Kipke and D. C. Martin, *Small*, 2010, **6**, 421–429.
241 R. D. Breukers, K. J. Gilmore, M. Kita, K. K. Wagner, M. J. Higgins, S. E. Moulton, G. M. Clark, D. L. Officer, R. M. I. Kapsa and G. G. Wallace, *J. Biomed. Mater. Res., Part A*, 2010, **95**, 256–268.
242 J. Xie, M. R. MacEwcm, S. M. Willerth, X. Li, D. W. Moran, S. E. Sakiyama-Elbert and Y. Xia, *Adv. Funct. Mater.*, 2009, **19**, 2312–2318.
243 R. D. Piner, J. Zhu, F. Xu, S. Hong and C. A. Mirkin, *Science*, 1999, **283**, 661–663.
244 D. S. Ginger, H. Zhang and C. A. Mirkin, *Angew. Chem., Int. Ed.*, 2004, **43**, 30–45.
245 W. C. M. Wang, R. M. Stoltenberg, S. H. Liu and Z. N. Bao, *ACS Nano*, 2008, **2**, 2135–2142.
246 J. C. Garno, Y. Y. Yang, N. A. Amro, S. Cruchon-Dupeyrat, S. W. Chen and G. Y. Liu, *Nano Lett.*, 2003, **3**, 389–395.
247 H. T. Wang, O. A. Nafday, J. R. Haaheim, E. Tevaarwerk, N. A. Amro, R. G. Sanedrin, C. Y. Chang, F. Ren and S. Pearton, *Appl. Phys. Lett.*, 2008, **93**, 143105.
248 B. W. Maynor, Y. Li and J. Liu, *Langmuir*, 2001, **17**, 2575–2578.
249 J. Chai, F. Huo, Z. Zheng, L. R. Giam, W. Shim and C. A. Mirkin, *Proc. Natl. Acad. Sci. U. S. A.*, 2010, **107**, 20202–20206.
250 B. Basnar, Y. Weizmann, Z. Cheglakov and I. Willner, *Adv. Mater.*, 2006, **18**, 713–718.
251 B. Basnar and I. Willner, *Small*, 2009, **5**, 28–44.
252 X. Duan, J. Zhang, X. Ling and Z. Liu, *J. Am. Chem. Soc.*, 2005, **127**, 8268–8269.
253 S. Lee, J. Park, Y. Cho, T. Park, Y. Kuk and J. Chung, *J. Vac. Sci. Technol., B*, 2007, **25**, 916–920.
254 W. M. Wang, M. C. LeMieux, S. Selvarasah, M. R. Dokmeci and Z. Bao, *ACS Nano*, 2009, **3**, 3543–3551.
255 H. H. Lu, C. Y. Lin, T. C. Hsiao, K. C. Ho, J. Tunney, D. Yang, S. Evoy, C. K. Lee and C. W. Lin, *Conf. Proc. IEEE Eng. Med. Biol. Soc.*, 2007, 2253–2256.
256 J. H. Lim and C. A. Mirkin, *Adv. Mater.*, 2002, **14**, 1474–1477.
257 M. Su, M. Aslam, L. Fu, N. Wu and V. P. Dravid, *Appl. Phys. Lett.*, 2004, **84**, 4200–4202.
258 B. W. Maynor, S. F. Filocamo, M. W. Grinstaff and J. Liu, *J. Am. Chem. Soc.*, 2001, **124**, 522–523.
259 H. Nakashima, M. J. Higgins, C. O'Connell, K. Torimitsu and G. G. Wallace, *Langmuir*, 2012, **28**, 804–811.
260 F. Huo, Z. Zheng, G. Zheng, L. R. Giam, H. Zhang and C. A. Mirkin, *Science*, 2008, **321**, 1658–1660.
261 F. Huo, G. Zheng, X. Liao, L. R. Giam, J. Chai, X. Chen, W. Shim and C. A. Mirkin, *Nat. Nanotechnol.*, 2010, **5**, 637–640.
262 A. L. Weisenhorn, P. Maivald, H. J. Butt and P. K. Hansma, *Phys. Rev. B: Condens. Matter Mater. Phys.*, 1992, **45**, 11226–11232.
263 E. Evans, *Annu. Rev. Biophys. Biomol. Struct.*, 2001, **30**, 105–128.
264 A. Sethuraman, M. Han, R. S. Kane and G. Belfort, *Langmuir*, 2004, **20**, 7779–7788.
265 S. L. McGurk, R. J. Green, G. H. Sanders, M. C. Davies, C. J. Roberts, S. J. B. Tendler and P. M. Williams, *Langmuir*, 1999, **15**, 5136–5140.
266 A. Gelmi, PhD thesis, unpublished.
267 A. B. Sanghvi, P. K. H. Miller, A. M. Belcher and C. E. Schmidt, *Nat. Mater.*, 2005, **4**, 496–502.
268 X. Y. Cui and D. C. Martin, *Sens. Actuators, B*, 2003, **89**, 92–102.
269 M. Berggren and A. Richter-Dahlfors, *Adv. Mater.*, 2007, **19**, 3201–3213.
270 J. N. Barisci, R. Stella, G. M. Spinks and G. G. Wallace, *Electrochim. Acta*, 2000, **46**, 519–531.
271 C. O'Connell, M. J. Higgins, H. Nakashima, S. E. Moulton and G. G. Wallace, *Langmuir*, 2012 (in press).